Structural Bioinformatics Analysis of Single Nucleotide Polymorphisms mapped to Cannabinoid Receptor 1

Syed Haneef

Master of Science (Biotechnology)

Vellore Institute of Technology (VIT) University, India

A thesis submitted in fulfilment of the requirements for the degree of

Master of Research (MRes)

June 2019

Department of Molecular Sciences

Macquarie University, Sydney, Australia

Abstract

G protein-coupled receptors (GPCRs) are key cell membrane-embedded receptor proteins, with critical roles in cellular signal transduction. In the era of precision medicine, understanding the role of variants on GPCR function is critical, especially from a pharmacogenomics view point. A computational method has been used to map deleterious non-synonymous single nucleotide polymorphisms (nsSNPs) to a GPCR in the endocannabinoid system, the human cannabinoid receptor 1 (CB1). Due to its central role in the endocannabinoid system, especially in the central nervous system, CB1 is an important drug target and its variability has implications for disease susceptibility and altered drug response. CB1 mutations were collated from relevant SNP databases and then computationally evaluated from neutral to deleterious. Mapping the variants on the CB1 structure showed the top twelve deleterious mutations were found to be either close to the ligand binding region or the G-protein binding site. From the top mutations, nine variants have clinical relevance, corresponding to phenotypic variations. Additionally, molecular docking analysis with a set of common ligands, variant structural analysis and, investigation of SNPs by molecular dynamics simulation, helped to understand the structural basis of variant pathogenicity.

Declaration

I declare that this thesis entitled "**Structural Bioinformatics Analysis of Single Nucleotide Polymorphisms mapped to Cannabinoid Receptor 1**" is representative of research work carried out by me under the guidance of Prof. Shoba Ranganathan, between July 2018 and April 2019 for the degree of Master of Research (MRes) in Molecular Sciences department at Macquarie University, New South Wales, Sydney, Australia.

The work presented here has not previously been submitted as part of requirements for a degree to any other university or institution other than Macquarie University. To the best of my knowledge, this submission is original, except where due reference is stated otherwise.

Syed Haneef

Acknowledgements

First and foremost, I would like to thank Allah the almighty for giving me the strength, knowledge, ability and opportunity to undertake this MRes research and to persevere and complete it satisfactorily. Without his blessings, this achievement would not have been possible.

I would like to acknowledge my indebtedness and render my warmest thanks to my supervisor, Prof. Shoba Ranganathan, for the patient guidance, encouragement and advice she has provided throughout my time as her student. I have been extremely lucky to have a supervisor who cared so much about my work, and who responded to my questions and queries so promptly.

I would also like to thank my co-supervisor, Prof. Mark Connor, from the Department of Biomedical Sciences, for discussions and valuable suggestions which have contributed greatly to the improvement of the work.

I extend my heartfelt thanks to my colleagues: Dr Abidali Mohamedali, Mr Dean Southwood, Ms Zainab Noor for their moral support and encouragement, and Mrs Amara Jabeen for her enormous help with molecular dynamics simulations.

My acknowledgement would be incomplete without thanking the biggest source of my strength, my family and friends in India. I would like to thank my parents and my brother, whose love and guidance are with me in whatever I pursue. Most importantly, I wish to thank my loving wife, Habeebunnisha, who provide unending inspiration.

Finally, I would like to thank Macquarie University not only for providing the International Macquarie University Research Excellence (iMQRES) scholarship to undertake this research, but also for giving me the opportunity to experience the Sydney life.

Table of Contents

List of Abbreviations

Δ^9-THC	Delta-9 tetrahydrocannabinol
2-AG	2-arachidonoyl glycerol
3D	3-Dimensional
β_2AR	β_2-adrenergic receptor
AEA	N-arachidonoyl-ethanolamine (Anandamide)
AMBER	Assisted Model Building with Energy Refinement
cAMP	Cyclic Adenosine Monophosphate
CB1	Cannabinoid Receptor 1
CB2	Cannabinoid Receptor 2
CBRs	Cannabinoid Receptors
CNR1	Cannabinoid Receptor 1 gene
CNS	Central Nervous System
C-terminus	Carboxyl-terminal
DRD2	Dopamine receptor D2
FAAH	Fatty Acid Amide Hydrolase
GPCR	G-protein coupled receptor
GRK	G-protein coupled receptor kinase
H-bond	Hydrogen Bond
ICM	Internal Coordinate Mechanics
MAPK	Mitogen-activated Protein Kinase
MD	Molecular dynamics
N-terminus	Amino-terminal
OPM	Orientations of Proteins and Membranes
PBCs	Periodic Boundary Conditions
PDB	Protein Data Bank
POPC	1-palmitoyl-2-oleoyl-sn-glycero-3-phosphocholine
PPM	Positioning of Proteins in Membrane
RMSD	Root Mean Square Deviation
RMSF	Root Mean Square Fluctuation
RoG	Radius of Gyration
SASA	Solvent Accessible Surface Area
SNPs	Single Nucleotide Polymorphisms
TM	Transmembrane

List of Tables

Chapter 3

List of Figures

Chapter 1

Chapter 2

Chapter 3

1. Introduction

1.1.Overview

Since early human history, the *Cannabis sativa,* a herbaceous plant commonly known as marijuana has remained important for medicinal, religious and recreational purposes (Iversen, 2009). The remarkable discovery of Δ^9-tetrahydrocannabinol (THC), the chief psychoactive compound from around 80 phytocannabinoids found in the cannabis plant (Ahmed et al., 2008; Elsohly & Slade, 2005; Radwan et al., 2008; Turner, Bouwsma, Billets, & Elsohly, 1980), became a popular recreational drug (Iversen, 2009). In the meantime, N-arachidonoyl-ethanolamine (AEA) an amide of arachidonic acid and ethanolamine generally called as anandamide and, 2-arachidonoyl glycerol (2-AG), a glyceryl ester, were discovered as the endogenous compounds with cannabimimetic action and were called as human endocannabinoids (Devane et al., 1992; Freund, Katona, & Piomelli, 2003; Mechoulam et al., 1995; Sugiura et al., 1995). The target receptors of these compounds were also identified in the human endocannabinoid system (ECS). Endocannabinoids have a major role in the human ECS, specifically in the central nervous system (CNS) (Lu & Mackie, 2016), with a neuromodulatory effect.

1.2.The endocannabinoid system

The human ECS is a complex signaling system responsible for many psychoactive effects in the body. It has two main cannabinoid receptors (CBRs) namely, labelled 1 (CB1) and 2 (CB2) (Pertwee et al., 2010). Additionally, it also has complete pathways for the biosynthesis and degradation of the endocannabinoids (Salzet, Breton, Bisogno, & Di Marzo, 2000). CB1 was the first cannabinoid receptor to be discovered (Devane, Dysarz, Johnson, Melvin, & Howlett, 1988) and cloned (Matsuda, Lolait, Brownstein, Young, & Bonner, 1990). Later, CB2 was identified and cloned (Munro, Thomas, & Abu-Shaar, 1993). CB1 is abundantly found in the brain, influencing different physiological and pathological conditions in the human body. It is found to be localized in the presynaptic neurons controlling neurotransmission release. Specifically, it is seen in γ-aminobutyric acid-(GABA)ergic, glutamatergic, and serotonergic neurons (Herkenham et al., 1991) as well as in brain glial cells (Mecha et al., 2015; Stella, 2009). CB1 is also sparsely seen in various other peripheral tissues including gastrointestinal, ocular, cardiovascular, immune, skeletal and even in liver and fat tissues (Busquets Garcia, Soria-Gomez, Bellocchio, & Marsicano, 2016). CB2 is distributed in the peripheral tissues particularly in the immune system (Dhopeshwarkar & Mackie, 2014; Svízenská, Dubový, & Sulcová, 2008). Apart from these

two CBRs, other orphan GPCRs, like GPR18, GPR19, GPR55 are discovered to act as the cannabinoid receptor (Atakan, 2012; Lauckner et al., 2008; Reggio, 2010; Ryberg et al., 2007). Evidently, CBRs are present in most tissues of the human body.

1.2.1. Cannabinoid receptors - the G protein-coupled receptors

Cannabinoid receptors are part of the G protein-coupled receptor (GPCR) superfamily with a conserved architecture of seven transmembrane (7TM) helical domains. The 7TMs are connected by three extracellular and three intracellular loops alternatively, with the N-terminus located outside the cell and the C-terminus inside it (**Figure 1.1**).

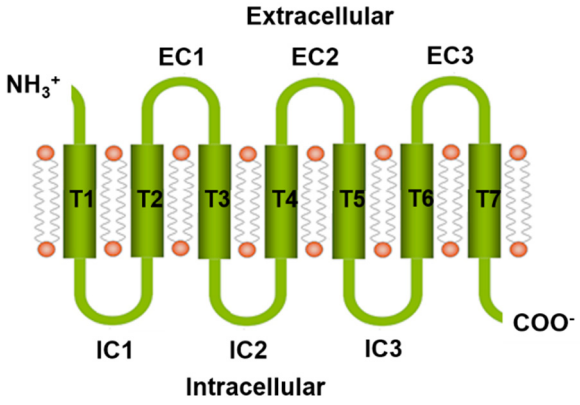

Figure 1.1. **GPCR topology.** The general topology of GPCRs, including cannabinoid receptor 1 (CB1).

The GPCR superfamily is classified into five sub-families: GRAFS (Glutamate, Rhodopsin, Adhesion, Frizzled/Taste2 and Secretin) (Fredriksson, Lagerström, Lundin, & Schiöth, 2003). The Rhodopsin clade (class A) is the largest GPCR sub-family, with 701 members, which are main drug targets for the pharmacological industries. The cannabinoid receptors are the rhodopsin-like lipid receptors, which fit into class A GPCRs (**Figure 1.2**). The CB1 and CB2 share 42% sequence identity (Shao et al., 2016).

These CBRs function *via* the GPCR signalling pathway, using adenylate cyclase (AC) (**Figure 1.3**) in the first instance, and then the mitogen-activated protein (MAP) kinase and the gating ion channels (Howlett et al., 2002). Generally, GPCR signalling is said to be biased, where different ligands acting on the same GPCR in the same tissue will give rise to different cellular responses (Ibsen, Connor, & Glass, 2017).

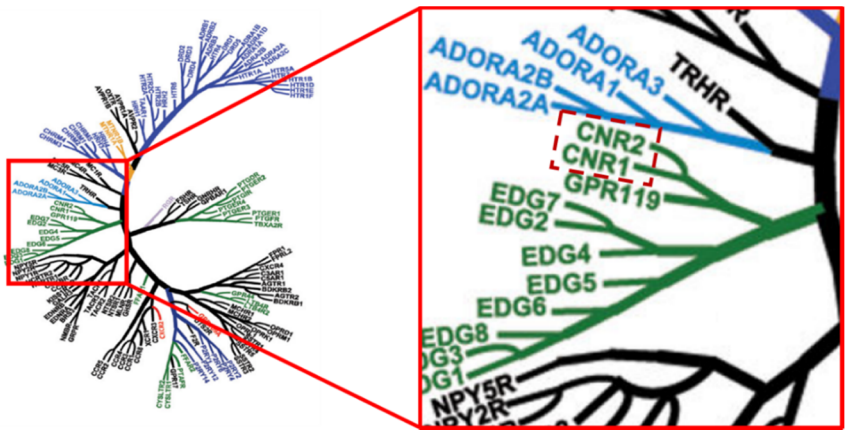

Figure 1.2. **Dendrogram classification of human GPCRs.** The cannabinoid receptors are shown in the magnified box (adapted from Lin, Sassano, Roth, & Shoichet, 2013).

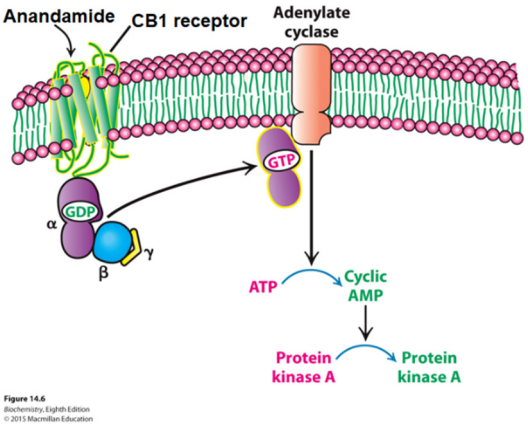

Figure 1.3. **Activation of CB1 receptor by G-protein pathway** (adapted from Berg, Tymoczko, Gatto & Stryer, 2015).

CBRs are involves in many pathological and physiological functions and, are responsible for various psychoactive effects in the human body (Katona & Freund, 2012). The human ECS functions as a retrograde signalling system, in which the signal arising from the post-synaptic neuron travels across the synapses, to bind to the pre-synaptic neuron (Ohno-Shosaku, Maejima, & Kano, 2001; Wilson & Nicoll, 2001). Endocannabinoids are allosteric enhancers or inhibitors, which mediate short-term and long-term neuronal plasticity at specific synapses. Anandamide acts as a retrograde messenger molecule after its synthesis in the post-synaptic neuron and controls the neurotransmitter release in the CB1-expressing pre-synaptic neuron (Egertová & Elphick, 2000). Besides CB1 and CB2, other nuclear receptors, such as the peroxisome proliferator-activated receptors (PPARs) (O'Sullivan, 2007; Pistis & Melis, 2010) and even ion channels have been reported to

interact with cannabinoids (Kano, Ohno-Shosaku, Hashimotodani, Uchigashima, & Watanabe, 2009; Zou & Kumar, 2018).

1.2.2. GPCRs: An area of continuing interest in the drug discovery

GPCRs have great pharmacological importance, around 50-60% of appropriate drugs have a therapeutic effect (Müller, 2000). Since 2006, the human ECS has emerged as the target for pharmacotherapy (Pacher, Bátkai, & Kunos, 2006). Further research on the identification of target compounds is ongoing, to harness the therapeutic potential of CBRs. To date, five different classes of cannabinoid compounds have been identified: i) classical cannabinoids, which are the natural constituents of cannabis, containing dibenzopyran derivatives (e.g., Δ^9-THC and Δ^8-THC) and their synthetic analogues (e.g., HU 210) (Howlett, Johnson, & Melvin, 1990); ii) non-classical cannabinoids, which are bicyclic and tricyclic analogues of Δ^9-THC without the pyran ring (e.g., CP-55,940) (Johnson & Melvin, 1986); iii) indoles with aminoalkylindoles (e.g., WIN-55,212) (Showalter, Compton, Martin, & Abood, 1996); iv) eicosanoids with arachidonic acid derivative (e.g., anandamide) (W. Devane et al., 1992), and v) antagonistic/inverse agonistic cannabinoids (e.g., SR141716A and AM251 for CB1, SR145528 and AM630 for CB2) (Console-Bram, Marcu, & Abood, 2012; Eissenstat et al., 1995; Howlett, 1995; Mechoulam et al., 1995; Rinaldi-Carmona et al., 1994, 1998; Xie, Melvin, & Makriyannis, 1996). The first cannabinoid antagonist to be studied was SR141716A (Rimonabant) (Rinaldi-Carmona et al., 1994), which is used to treat metabolic syndrome and obesity (Pagotto & Pasquali, 2005; Pagotto, Vicennati, & Pasquali, 2005; Wierzbicki, 2006).

1.2.3. Emerging strategies in targeting the cannabinoid receptors

CB1 in the human ECS has greater pharmacological importance compared to CB2. CB1 targets the CNS, by influencing pain, appetite, anxiety, depression, learning and memory skills, stroke, schizophrenia, multiple sclerosis, epilepsy, nicotine addiction, neurodegeneration and other conditions like diabetes, obesity, Alzheimer's disease, Huntington's disease and Parkinson's disease. It is also responsible for physiological and pathological conditions in the peripheral tissues involving energy metabolism, cardiovascular conditions, reproductive functions, inflammation, glaucoma, cancer, liver and musculoskeletal disorders. In summary, CB1 shows a wide range of biological activities in the human body (Cravatt & Lichtman, 2004; Di Marzo, Stella, & Zimmer, 2015; Fernández-Ruiz, Romero, & Ramos, 2015; Ibsen et al., 2017; Iversen, 2003; Maccarrone et al., 2015; Miller & Devi, 2011; Pacher et al., 2006; Roger G. Pertwee, 2002; Pryce & Baker,

2015). As CB2 is expressed in peripheral tissues, its neurological effect is not clearly understood (Atwood & Mackie, 2010; Gong et al., 2006). However, a recent study has been reported that CB2 is involved in neuronal firing (den Boon et al., 2012).

The activation of CB1 in the cerebellar granule cells (CGCs) results in decreased activation of neuronal nitric oxide synthase (NOS), affecting brain function (Hillard, Muthian, & Kearn, 1999). While CB1 has great pharmacological importance, the systematic activation of CB1 receptor produces some undesired side effects, which are practically unavoidable. The CB1 receptor's mode of action is known based on biochemical experimental evidence.

1.3.Single Nucleotide Polymorphisms (SNPs)

Single nucleotide polymorphisms (SNPs) are mutations produced by a single base change in the DNA sequence (**Figure 1.4**). There are roughly 10 million SNPs in the entire human genome. SNPs which are very close to a particular gene, act as a biological marker for that gene. SNP variations can be seen in the non-coding regions, as well as in the coding regions of the gene. Variations in coding regions are classified into synonymous and non-synonymous mutations. Synonymous mutations are the silent substitutions which do not change the encoded amino acid. Non-synonymous mutations are further classified into missense and nonsense mutations. Missense mutations are the point substitutions which change the encoded amino acid, while nonsense mutation codes a stop codon, thereby truncating the resultant protein sequence.

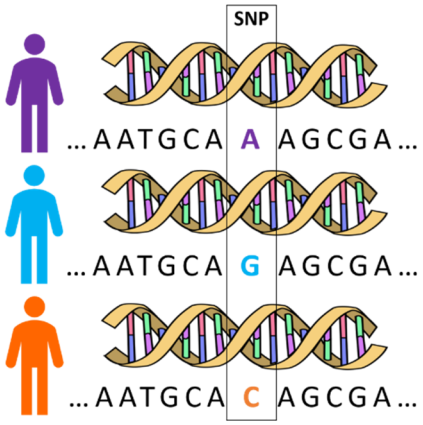

Figure 1.4. **Single Nucleotide Polymorphisms (SNPs)**.

1.3.1. SNPs in GPCRs

A large number of variants are observed in GPCRs, with an average of four common and 128 rare variants noted for each receptor (Villanueva, 2018). More than 160 SNPs have

been reported for the β_2-adrenergic receptor (β_2AR), of which three SNPs are found to be clinically significant. Mutations in GPCRs can result in altered signalling or impaired G-protein binding. Such changes are known to contribute to hyper- and hypothyroidism, nephrogenic diabetes as well as carcinoma (Schöneberg et al., 2004). Clinically significant SNPs in GPCRs are vulnerable to disease, and show adverse drug responses. Rhodopsin variants have a phenotypic effect causing retinitis pigmentosa and congenital night blindness (Daiger, Sullivan, & Bowne, 2013). The V209M and F220C mutants in the rhodopsin (Rho) receptor are responsible for the condition, retinitis pigmentosa, by altering the receptor folding and cellular trafficking (Mallory et al., 2018). Gain- and loss-of-function mutations are known to cause dysfunction or dysregulation of GPCRs. Endocrine disorders such as congenital gonadotrophin deficiency, are attributed to loss-of-function GPCR mutations in *KISS1R*, *TACR3*, *GNRHR* and *PROKR2* genes (Fukami, Suzuki, Igarashi, Miyado, & Ogata, 2018). Cys-Cys chemokine receptor 6 (CCR6) missense variants exhibit a loss-of-function effect by decreasing G-protein signaling (Julian, Gao, Harwood, Beinborn, & Kopin, 2017). Experimental assays show that the variants of μ-opioid receptor and cholecystokinin-A receptors display an altered drug response (Hauser et al., 2018).

1.3.2. SNPs in cannabinoid receptor 1

Mutations in the CB1 receptor, are likely to alter its ligand recognition and binding affinity. CB1 mutations alter the G-protein specificity and, selectively disrupt the G-protein signalling (Roche, Bounds, Brown, & Mackie, 1999; Ulfers et al., 2002). CB1 mutations are apparent in conditions like eating disorders, including anorexia nervosa and bulimia nervosa (Monteleone et al., 2009) and also known to affect the happiness level and mood (Chakrabarti, Kent, Suckling, Bullmore, & Baron-Cohen, 2006; Matsunaga et al., 2014), as well as a broad spectrum of neurological disorders (Smith, Stanley, Foss, Boles, & McKernan, 2017). Genetic variations in the human ECS give a different response to Cognitive Behaviour Therapy (CBT) for anxiety disorder (Lester et al., 2017). Polymorphisms in *CNR1* gene, which codes for CB1, are found to be associated with weight gain in Schizophrenia patients of European origin (Tiwari et al., 2010) and susceptible to the hebephrenic-type schizophrenia (Ujike et al., 2002). In another study, specific CB1 receptor gene variations correlate with a high risk for obesity in the European population (Benzinou et al., 2008). Genetic variations in the CB1 receptor is also found to increase the risk of type-2 diabetes and define obesity phenotypes in European men (Russo et al., 2007; Scheen, 2007). Post-translationally modified CB1 receptor, by palmitoylation, fails to achieve membrane localisation and subsequently, signalling (Oddi et al., 2012). T210 mutation in

CB1 is known to influence shuffling of active and inactive receptor state, while mutations in the CB1 DRY (Asp-Arg-Tyr) motif (a conserved GPCR sequence motif) have increased its affinity for agonist ligands and decreased for antagonist ligands (D'Antona, Ahn, & Kendall, 2006; D'Antona, Ahn, Wang, et al., 2006). F238L point mutation in the CB1 receptor showed an increased axonal polarization (Wickert et al., 2018). CB1 SNPs rs806368, rs806371, and rs2180619 are associated with modulation of personality and psychiatric conditions (Yao et al., 2018).

In the Turkish population, the *CNR1* and the *DRD2* (dopamine receptor D2) gene interaction study revealed that polymorphisms in these genes are responsible for the risk factors in cannabis addiction (Isir, Baransel, & Nacak, 2016). Variants involved in the cannabis usage disorders (CUDs) suggested that CB1 is associated with FAAH (Fatty Acid Amide Hydrolase) and shows marijuana-related problems in Mexican Americans (MAs) and irritable bowel syndrome (IBS) in Chinese patients, besides drug-related behaviour and weight gain (Bidwell et al., 2013; Jiang, Nie, Li, & Zhang, 2014; López-Moreno, Echeverry-Alzate, & Bühler, 2012; Melroy-Greif, Wilhelmsen, & Ehlers, 2016; Palmiero Monteleone, Milano, Petrella, Canestrelli, & Maj, 2010). SNPs in *CNR1* and peroxisome proliferator activator receptor-α (PPARA) have been linked to schizophrenia (Costa et al., 2013). CB1 SNP rs2023239 shows a protective effect against major depressive disorder (MDD) (Icick et al., 2015). A *CNR1* haplotype showed abnormal lipid homeostasis (Baye et al., 2008). *CNR1* variations rs6454674 and rs806368 together were found to control drug and alcohol dependence in European Americans (EAs) (Zuo, Kranzler, Luo, Covault, & Gelernter, 2007). Specific CB1 variants even showed decreased cannabis dependence symptoms in adults (Hopfer et al., 2006) while there was no association of endocannabinoid genes in bipolar disorder in Sardinian individuals (Pisanu et al., 2013). All these reported studies are based on limited cohort sizes and a large-scale study is required to completely understand mutation effects in CB1.

1.4.Structure of cannabinoid receptor 1

The human CB1 receptor is encoded by the *CNR1* gene with 472 amino acids. *CNR1* is localized in the human chromosome 6 exactly at the position 6q14–q15 (Hoehe et al., 1991). It spans 26.1 kb with four exons (Laprairie, Kelly, & Denovan-Wright, 2012; Zhang et al., 2004). CB1's binding pocket has been established by X-ray crystallographic structures. The first study (Hua et al., 2016) reports CB1 receptor in the inactive conformation with a bound stabilizing antagonist (AM6538), at a resolution of 2.8Å (PDB ID: 5TGZ). The second structure is of the inactive receptor, with the bound inhibitor, taranabant, resolved at 2.6 Å

PDB ID: 5U09 (**Figure 1.5**) (Shao et al., 2016), showing the involvement of the N-terminal segment of CB1 and the membrane-proximal region (conserved within the lipid-binding GPCR sub-family) in the ligand-binding cavity. Two more CB1 structures in an active conformation with agonist-bound complex with tetrahydrocannabinol (AM11542) (PDB ID: 5XRA) and hexahydrocannabinol (AM841) (PDB ID: 5XR8) (Hua et al., 2017) uncovers the CB1 activation mechanism and aids in understanding the binding pattern of cannabinoids. Recently, a cryo-EM structure of the CB1-G_i protein complex (PDB ID: 6N4B) (Krishna Kumar et al., 2019) with 3Å resolution is available, with a bound potent agonist MDMB-Fubinaca. This study describes the toggle switch activation mechanism, which is responsible for GPCR activation. However, these structures lack the N- and C-terminal residues as well as part of the intracellular loop 3 (IC3), which is involved in G-protein binding.

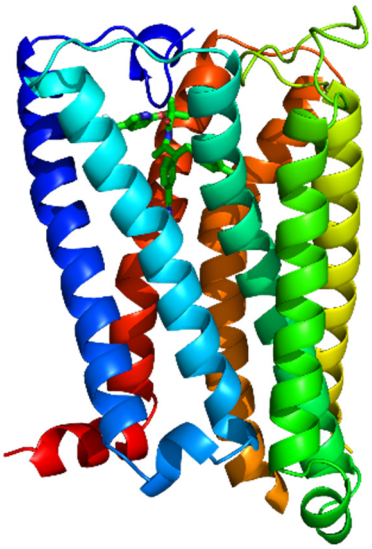

Figure 1.5. **Experimental cannabinoid receptor 1 structure.** An X-ray crystal structure of cannabinoid receptor 1 (coloured in the rainbow spectrum with the N-terminus in blue and the C-terminus in red) bound with the inhibitor taranabant (green; in stick representation). Helix 8 is part of the carboxy terminal and not embedded in the membrane.

Such structural understanding is helpful for designing CB1 specific ligands, with enhanced pharmacological properties. Compared to antagonists, agonist ligands have a much greater influence on the CB1 receptor signalling. Thus, any change in the CB1 ligand binding site, due to ligand specificity or affinity, the tissue specificity of the receptor or mutations, will therefore have an immense effect on CB1 function. Mutations will also influence the structural conformation of the CB1 receptor, affecting activation.

1.5.Aims and objectives

The overall aim of this study is to map naturally occurring SNPs to CB1 structure, to understand how mutants will affect CB1 function, using bioinformatics methods.

My specific aims are:

1. to collect SNPs in CNR1 gene of the CB1 receptor from the public repository databases and to prioritize the collected SNPs for their disease pathogenicity by using *in silico* prediction tools and identify potential highly deleterious SNPs.
2. to map these highly deleterious SNPs to the 3D structure of CB1, to identify the mutational hotspots in the CB1 receptor and to correlate mutational effects with available genotype-phenotype data.
3. to apply molecular docking to understand the mutational effect upon ligand binding. Variant structural analysis of the CB1 receptor in the inactive- and active-state conformations will be carried out to obtain detailed structural implications caused by the mutations. Molecular dynamics simulations of selected SNPs will be used to understand the real time effect of mutations on the CB1 receptor structure and function.

2. Methods

The importance of endocannabinoids in numerous physiological and pathological processes has recently been reviewed (Hourani & Alexander, 2018), with several ligands targeting different paths of the CNS. However, the phenotypic variation due to SNPs has not been studied in detail. It is therefore crucial to map the SNPs to the CB1 structure, especially the ligand-binding cavity, to correlate the SNP consequences at the protein level to the observed phenotypic effects. There is an urgent need to discover the mutational hotspots in the CB1 receptor and map them on the CB1 structure. Such comparative structural analysis of the mutations will help us to understand better about the genotype-phenotype correlation (Huynh, Khan, & Ranganathan, 2011; Khan & Ranganathan, 2009).

2.1.SNP Mining and Prediction

Advance sequencing methods have increased the identification of nonsynonymous missense mutations, with their functional consequence characterized computationally, using protein structure (George et al., 2014), and as applied to GnRHR, KISS1R, PROKR2, and TACR3 GPCRs (Min et al., 2016). CB1 variants have been yet to be structurally analysed and the following sections describe the general approach for mapping GPCR variants onto structure, to gain an insight into their functional consequences. SNPs in the coding regions of CB1 receptor gene *CNR1*, were collected from the major public data repositories, dbSNP (Sherry et al., 2001) and GPCRdb (Pándy-Szekeres et al., 2018). CB1 had a total of 248 SNPs. 190 missense mutations (excluding synonymous and stop codon mutations) within the coding region of the *CNR1* gene (Supplementary Table 1), were predicted to have a functional effect, using prediction tools such as PredictSNP (Bendl et al., 2014) and PON-P2 (Niroula, Urolagin, & Vihinen, 2015). Meta-SNP (Capriotti, Altman, & Bromberg, 2013) includes the individual tools of SIFT, PhD-SNP, SNAP, and PANTER, which are also present in PredictSNP and PON-P2. The accuracy of the most widely used prediction tools is in the range of 60-82% (Thusberg, Olatubosun, & Vihinen, 2011), providing rapid characterization of variants.

2.2.Homology Modelling

Three dimensional (3D) structural analysis of CB1 receptor, in the inactive- and active-state, helps in understanding the functional consequences of SNPs. There are four CB1 X-ray crystallographic structures deposited in the PDB database (Berman et al., 2000). However, these structures are all missing the highly variable IC3 loop which interacts with G-protein during signaling. Hence, the complete CB1 receptor structure was modelled using

MODELLER version 9.20 (Webb & Sali, 2016). Comparative modelling has three sequential steps, with fold assignment, target-template alignment and model building (**Figure 2.1**), followed by model evaluation.

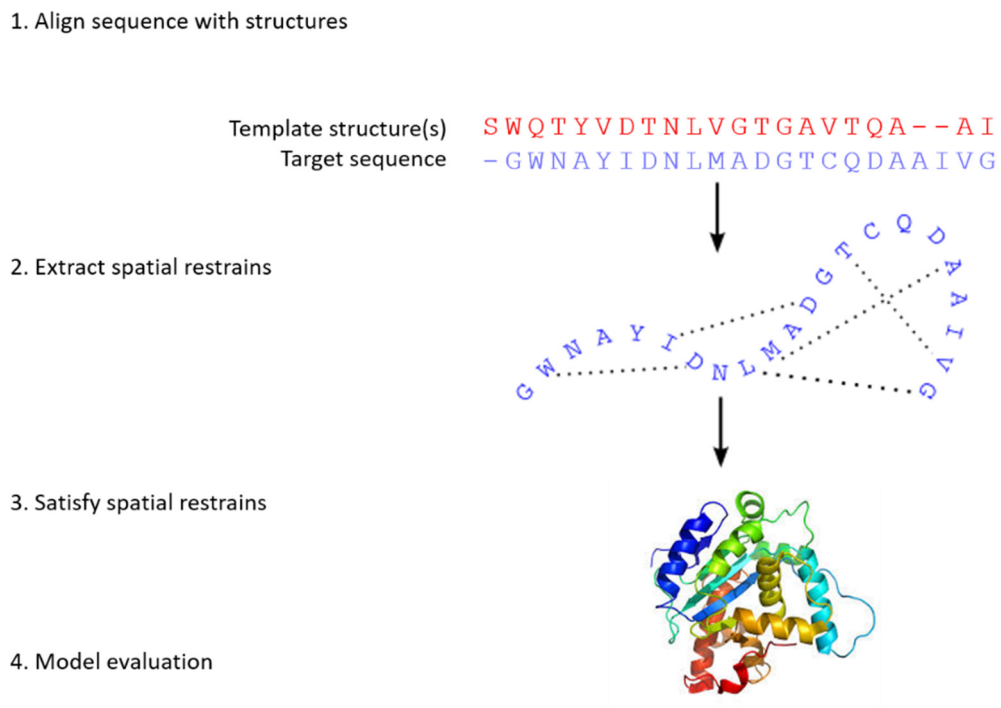

Figure 2.1 MODELLER workflow. An automated approach implemented by MODELLER for comparative protein structure modelling (adapted from MODELLER manual Release 9.20, r11208).

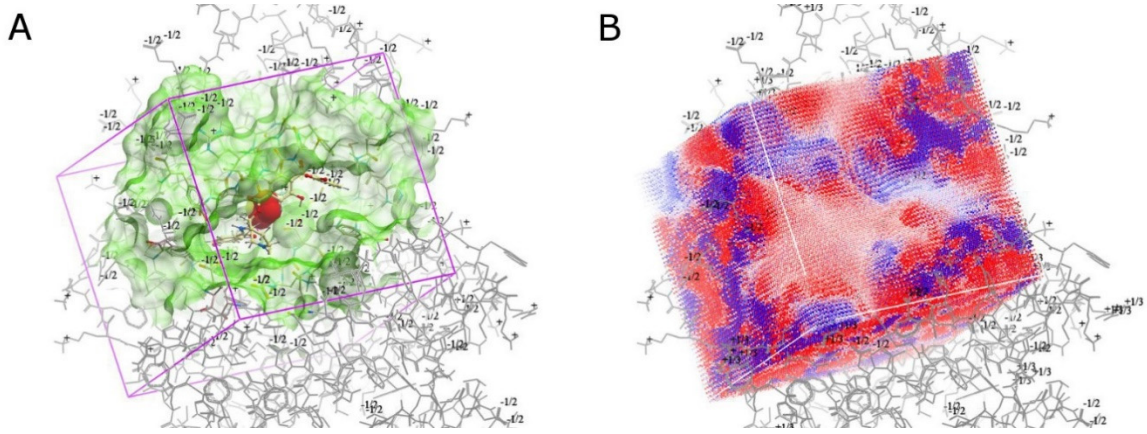

Figure 2.2 ICM grid setup for sampling ligand binding site. (A) A rectangular grid box (purple color) with 0.5 Å spacing, which represents the region where maps will be generated is shown with (B) displaying the calculated grid potential maps.

2.3.Molecular Docking

Molecular docking is a computational method to predict the binding mode of a small-molecule ligand to a given protein receptor. Atomic-level protein-ligand interactions from molecular docking, can be evaluated for deciphering GPCR drug binding patterns (Kitchen, Decornez, Furr, & Bajorath, 2004). ICM software was used to perform molecular docking (Neves, Totrov, & Abagyan, 2012), using the induced fit (flexible) mode. Flexible docking in ICM uses Monte Carlo simulations for global optimization of ligand internal coordinates provided in the grid potential maps calculated for the ligand binding site. A rectangular box with 0.5 Å is generated as the grid space centred at the ligand binding site (**Figure 2.2**). The use of such grid maps reduces the calculation time for ligand sampling. The ICM pocket finder analyses the protein structure to locate cavities and clefts. The pocket finder was used to identify the binding site in CB1.

2.4.Molecular Dynamics

Protein dynamics can be analyzed at the atomic level through molecular dynamics simulations, also known as the "computational microscope" (Dror, Dirks, Grossman, Xu, & Shaw, 2012). Molecular dynamics (MD) simulations are used to understand the structure of protein and interaction of molecules, and has been used for GPCR structure-based drug design (Sensoy, Almeida, Shabbir, Moreira, & Morra, 2017). The different steps involved in preparing the CB1 structure for MD simulations are briefly described below.

2.4.1. Receptor preparation

The orientation of all the structures with reference to the membrane was determined by the Positioning of Proteins in Membrane (PPM) server of the Orientations of Proteins and Membranes (OPM) database (Lomize, Pogozheva, Joo, Mosberg, & Lomize, 2012). The oriented structures were embedded in a fully hydrated POPC (1-palmitoyl-2-oleoyl-sn-glycero-3-phosphocholine) lipid bilayer using the CHARMM-GUI Membrane builder (Jo, Kim, & Im, 2007; Jo, Kim, Iyer, & Im, 2008; Wu et al., 2014) (**Figure 2.3**).

The protein-membrane system was then solvated using the TIP3 water model (Jorgensen, Chandrasekhar, Madura, Impey, & Klein, 1983) and 0.15M NaCl ions were placed using the Monte Carlo method. The endocannabinoid, anandamide, was selected as the ligand, in order to under mutational effects under physiological conditions. The ligand's force field parameters were obtained from the ParamChem (Vanommeslaeghe & MacKerell, 2012; Vanommeslaeghe, Raman, & MacKerell, 2012) with CHARMM General Force Field (CGenFF) (Vanommeslaeghe et al., 2010).

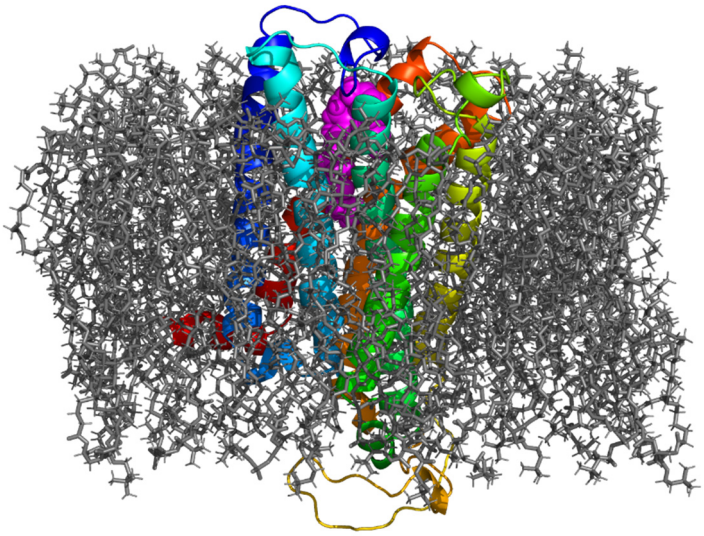

Figure 2.3 Lipid embedded CB1 structure. A typical structure of CB1 receptor (coloured in the rainbow spectrum with the N-terminus in blue and the C-terminus in red) bound with the endogenous ligand anandamide (magenta; in sphere representation) embedded in the fully hydrated POPC lipid bilayer (grey; in stick representation). Water molecules and NaCl ions are not shown for clarity.

2.4.2. Molecular dynamics simulation

All MD simulations in this study were performed using AMBER (Assisted Model Building with Energy Refinement) 16 package (Case et al., 2005).

Amber force field:

In general, Amber force field (Cornell et al., 1995) is described as follow:

$$E_{total} = \sum_{bonds} K_b(l - l_0)^2 + \sum_{angles} K_a(\theta - \theta_0)^2 + \sum_{torsions} \frac{V_n}{2}[1 + \cos(n\emptyset - \gamma)] + \sum_{i<j} \left[\frac{A_{ij}}{R_{ij}^{12}} - \frac{B_{ij}}{R_{ij}^{6}} - \frac{q_i q_j}{\varepsilon R_{ij}}\right]$$

The first three summations represent intramolecular measures, *i.e.* bond length, angle, and torsion, respectively, while the last summation represents the interatomic interaction, including van der Waals and electrostatic interactions, based on a 6-12 interaction potential.

MD simulations were typically computed under periodic boundary conditions (PBCs). The periodic boundary conditions were applied in all directions. An overall cutoff of 10Å was set for both the van der Waals and electrostatic interactions (short-range interactions) and the covalent interactions involving heavy and hydrogen atoms (long-range

interactions), using the Particle Mesh Ewald (PME) (Darden, York, & Pedersen, 1993) and SHAKE (Ryckaert, Ciccotti, & Berendsen, 1977) algorithms. PBCs can be represented as a cubic box of particles which is simulated in all directions. A 2D project of the box is shown in **Figure 2.4**, where the central box has eight nearest neighbours. If a particle exits the box during the course of the simulation, it is replaced by a particle from the opposite side. Thus, the number of particles within the box remains constant.

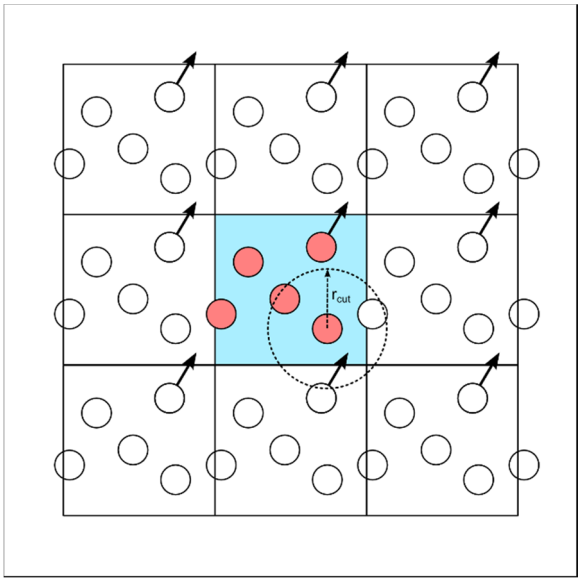

Figure 2.4 Periodic boundary conditions (PBCs). If a particle exits the box, it is replaced by a particle from the opposite side as represented by the arrow (adapted from Allen, 2004).

The coordinate and topology files for the ligand anandamide was prepared using the antechamber module of Amber. Another module, Tleap was used to create the coordinate and topology files of the protein and also to create the protein-ligand complex for running MD simulations. The amber ff14SB molecular mechanical force field (Maier et al., 2015) for the protein, the general amber force field (gaff) (Wang, Wolf, Caldwell, Kollman, & Case, 2004) for the ligand and the amber Lipid14 force field (Dickson et al., 2014) for the lipid bilayer were employed for simulations. The TIP3 water model was represented using TIP3P. All systems were neutralized by adding either Na^+ or Cl^- ions based on the system's actual charge. A rectangular box was defined around the Amber coordinate system. The final system dimension was approximately 75Å × 75Å × 120Å.

The entire system was energy minimized to avoid any steric clashes. The system was carefully energy minimized using a sequence of three steps by following the Steepest Descent algorithm coupling a total of 5000 iterations. In step one, only the solvents were minimized. The backbone restraints were removed for the protein complex in step two and

finally, no restraints were set and the entire system was energy minimized. Successively the entire system was gradually heated from 0 to 310 K over a 100ps period and followed by a 250ps simulation to equilibrate the entire system. Finally, the prepared system setup was used for the production of molecular dynamics simulations. It was carried out for 100ns (1μs) time period without any restraints. The simulations were carried out and the simulation coordinates were saved for every time step of 1ns. The simulation steps were consistent with time frames reported for CB1 simulations with other ligands (Jung, Cho, & Yu, 2018).

2.4.3. MD Simulation Analysis

After the production of molecular dynamics simulations, the trajectory data was analyzed using CPPTRAJ (Roe & Cheatham, 2013). The trajectories were analyzed for stability and fluctuations of the systems. In order to measure the energy stability of the protein, root mean square deviation (RMSD) was calculated. This gives an idea of the closeness between three-dimensional structures. The spatial fluctuation of residues was analyzed by calculating the root mean square fluctuation (RMSF). This helps to understand how residues behave in different protein conformations on an average. The global dimension of the protein was calculated by the radius of gyration (RoG). It is the measure of mass-weighted RMS distance between atoms from their centre of mass. Furthermore, the total number of hydrogen bonds formed in protein during the simulation was also calculated. The conditions to measure H-bonds are based on limits in the hydrogen-donor-acceptor angle (30°) and their distance (0.35nm). Considering the NH and OH groups as the donors and the O and N atoms as the acceptors (Baker & Hubbard, 1984). The Solvent-accessible surface area (SASA) was also calculated. The solvation in the protein environment is triggered by the contact of the solvent with the protein surface. This is the driving force for protein folding and stability (Eisenberg & McLachlan, 1986). These solvent accessible residues are buried in the hydrophobic region. The solvation energy can be calculated using implicit solvent models in molecular dynamics simulation (Ferrara, Apostolakis, & Caflisch, 2002). SASA is measured as probe rolls over the protein surface in such models. In AMBER, the LCPO method (Weiser, Shenkin, & Still, 1999) is used to calculate the SASA. To compare the RMSD, RMSF, RoG, the number of H-bonds and SASA in the wild type structure and the variants structure in their inactive- and active-state conformations, the values were plotted using the XMGRACE (Graphing, Advanced Computation, and Exploration) program (Turner, 2005). The binding free energy of CB1-ligand complexes was calculated using the MMPBSA (Molecular Mechanics Poisson-Boltzmann surface area) approach (Gohlke, & Case, 2004).

3. Results

3.1.Deleterious SNP Prediction

CB1 had a total of 248 SNPs of which 190 missense mutations (excluding synonymous and stop codon mutations; listed in Supplementary Table 1) within the coding region of the *CNR1* gene, were computationally analyzed for pathogenicity using PredictSNP and PON-P2. As the number of predicted deleterious SNPs is large, we prioritized mutations by setting a cutoff score of >75% confidence (from PredictSNP) and >75% pathogenicity probability (from PON-P2) of the amino acid substitutions. Meta-SNP (Capriotti, Altman, & Bromberg, 2013) was not considered, as the subset tools in this method were also incorporated into the PredictSNP server, although all three methods were used equally by Tandale et al. (Tandale, Joshi, & Sengupta, 2016). Based on these cutoff values, 18 mutations were found to be deleterious, of which 12 had structural information (**Table 3.1**), while R14H and R14L are in the missing N-terminal region, and H302P, R311C, R331Q and R331W are in the missing intracellular loop 3 (IC3). Below the cutoff threshold, a total of 38 variants had borderline predictive score between 50% and 75%, from which F174A and L193A were reported to be the main contact residues (Shim et al., 2011), for the synthetic ligand, HU-210. A total of 140 SNPs were filtered out, as they were not predicted to be deleterious by both the prediction tools. Importantly, the highly deleterious SNPs do not contain a single residue listed in the three predicted allosteric pockets of CB1 (Sabatucci, Tortolani, Dainese, & Maccarrone, 2018).

The prioritized SNPs were mapped to the CB1 receptor structure to highlight the mutational hotspots (**Figure 3.1**). It is interesting to note that the experimental studies listed in Table 3.1 (Chin, Lucas-Lenard, Abadji, & Kendall, 1998; Fay, Dunham, & Farrens, 2005; McAllister et al., 2002; Shim, 2010; Shim, Bertalovitz, & Kendall, 2011) report three different agonists (WIN 55,212-2, CP55,940, HU-210) and an antagonist (SR141716), making extrapolation of results between the studies difficult. The best-known ligands for CB1 are shown in **Figure 3.2**.

Additionally, the structural consequences of the 12 significant SNPs listed in (Table 3.1), was carried out by mapping to the inactive- (PDB ID: 5U09) and active-state (PDB ID: 5XRA) structures of the CB1 receptor, followed by docking a common selected set of ligands, comprising agonists (the endocannabinoid anandamide and THC); an inverse agonist, rimonabant and an antagonist, surinabant.

Table 3.1 Predicted list of deleterious CB1 SNPs by computational tools. Variants in bold are experimentally confirmed to have functional change in the receptor.

S.No	SNP ID	Variant	PredictSNP (Confidence)	PON-P2 (Probability)	Ligand Tested	Functional Change	Reference
1	GPCRdb	**D163E**	Deleterious (76%)	Pathogenic (0.91)	WIN 55,212-2 (agonist)	Loss of G-protein signaling	(Shim, 2010)
2	GPCRdb	**D163N**	Deleterious (76%)	Pathogenic (0.91)			
3	rs748199661	D163Y	Deleterious (87%)	Pathogenic (0.92)	-	-	-
4	GPCRdb	**K192E**	Deleterious (87%)	Pathogenic (0.88)	CP55, 940 (non-classical agonist)	Attenuates receptor activation	(Chin et al., 1998)
5	GPCRdb	**C257A**	Deleterious (87%)	Pathogenic (0.84)	SR141716 (antagonist)	Complete loss of ligand binding	(Fay et al., 2005)
6	GPCRdb	**C264A**	Deleterious (76%)	Pathogenic (0.82)			
7	GPCRdb	**Y275F**	Deleterious (87%)	Pathogenic (0.77)	CP55, 940 (non-classical agonist)	Inhibition of cAMP is slightly reduced	(McAllister et al., 2002)
8	rs757316503	W299R	Deleterious (87%)	Pathogenic (0.92)		-	-
9	rs763132752	R336C	Deleterious (87%)	Pathogenic (0.93)		-	-
10	GPCRdb	**C355A**	Deleterious (76%)	Pathogenic (0.84)	WIN 55,212-2 (agonist)	No loss	(Shim, 2010)
11	GPCRdb	**M363A**	Deleterious (76%)	Pathogenic (0.96)	HU-210 (agonist)	Reduced potency for G-protein & Ligand binding	(Shim et al., 2011)
12	rs907130013	*Y397C	Deleterious (87%)	Pathogenic (0.95)	-	*Y397 contributes to breakage of ionic lock	(Shim, 2010)

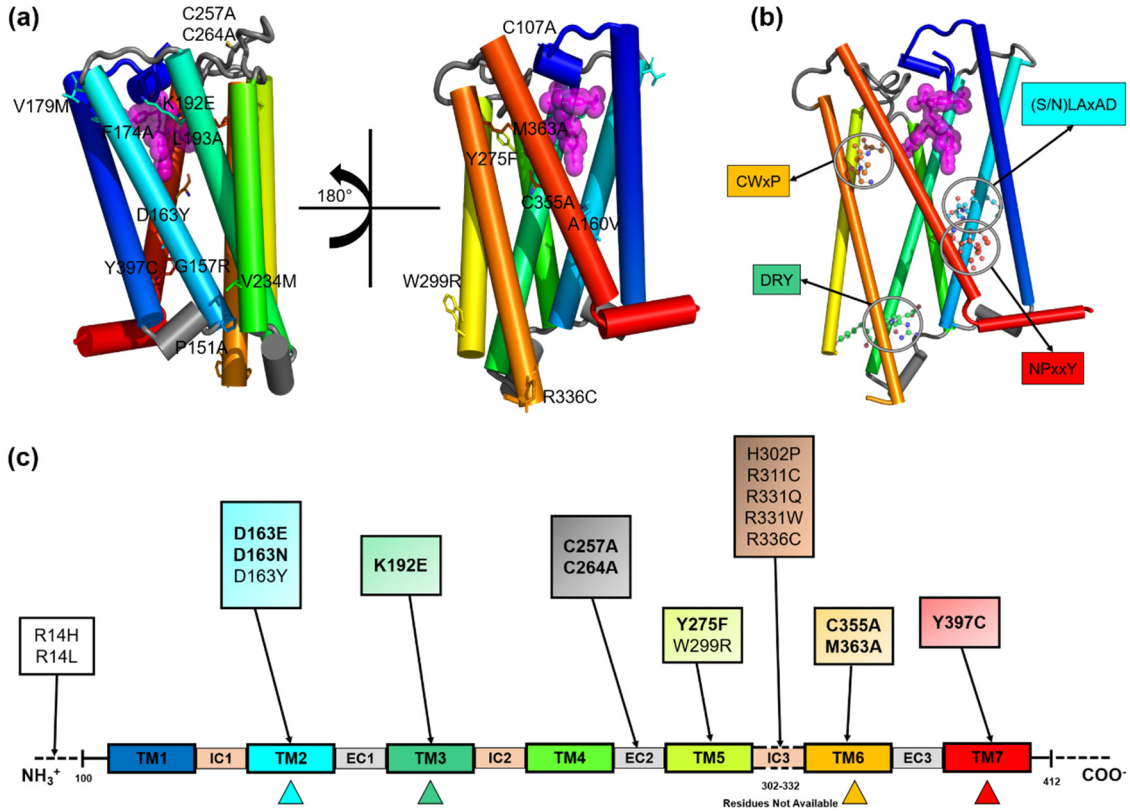

Figure 3.1 CB1 variant sites. A cylindrical tube representation of the human CB1 receptor helices (PDB ID: 5U09) coloured in the rainbow spectrum with the N-terminus in blue and the C-terminus in red. (**a**) Front and back views. The positions harbouring the variants are rendered in stick representation coloured by their atom type and are labelled. **(b)** 3D location of sequence motifs: (S/N)LAxAD (in cyan), DRY (in green), CWxP (in orange) and NPxxY (in red). (**c**) Mutational hotspots mapped on the human CB1 receptor sequence. Experimentally confirmed variants are shown in bold font. Regions without structural information at the N-terminus, the C-terminus and in the IC3 loop are represented by dotted lines. The triangles mark the positions of the four motifs or microswitches, described in **(b)**.

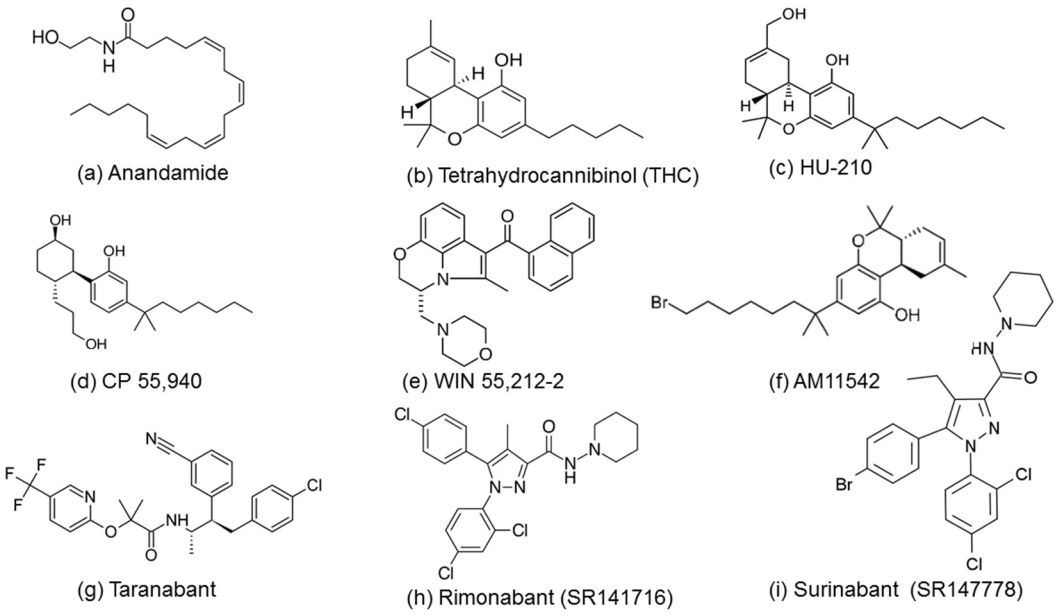

Figure 3.2 Human CB1 receptor ligands. (a)-(f) are agonists, (g) and (h) are inverse agonists and (i) is an antagonist.

We first mapped the nine SNPs with experimental information (Table 3.1), to check if structural analysis could provide explanations for the observations reported, and then proceeded with the analysis of three SNPs with no experimental information. Interesting SNPs were further analysed by molecular dynamics (MD) simulations, with the endocannabinoid, anandamide bound to the lipid-embedded CB1 receptor.

3.2.Homology Modelling

In order to compare the inactive- and active-state CB1 receptor structures in their native state (WT) and mutant forms, we need to generate variant structural models that are conformationally energy minimized, rather than simply replace a side chain, without optimizing the entire structure. Hyunh et al. successfully used such an approach to correlate genotypic changes with phenotype (Huynh, Khan, & Ranganathan, 2011). Furthermore, to make comparisons between the active and inactive structures, the same ligands should be docked into the active site, as the first step of structural analysis. The available ligand-bound CB1 structures of the inactive (PDB ID: 5U09, with bound taranabant) and the active (PDB ID: 5XRA with bound AM11542) conformations were used as template structures for homology modeling, using MODELLER version 9.20 (Webb & Sali, 2016). Five structures for each conformation of the CB1 receptor were generated for each variant in Table 3.1 and the structure with the lowest DOPE score (discrete optimized protein energy) was selected. All structures were annealed using in-built Monte Carlo simulations, as reported in a recent

study on the GPCR, 5-HT1A, and agonists leading to the discovery of two potentially active ligands through virtual screening. (Warszycki, et al., 2017). With only single amino acid change, all the CB1 models developed in this study had an RMSD value of <1 Å.

3.3.Molecular Docking

The docking protocol followed was the induced fit (flexible) mode in ICM (Totrov & Abagyan, 1997). In order to verify the applicability of the docking protocol, the original ligands in the CB1 structures were re-docked to their respective PDB structures. The ICM pocket finder was used to identify the binding site in different CB1 structures consistently. The binding site with the high DLID score was selected and it was defined for docking. For the inactive CB1 structure (5U09), taranabant was re-docked with an RMSD of 0.23 Å, while for the active structure (5XRA), AM11542 was re-docked with an RMSD of 0.19 Å. We then docked selected set of common ligands (anandamide, THC, rimonabant and surinabant) to the orthosteric binding site of the inactive- and active-state native (WT) and mutant structures of CB1 receptor, using the approach described above for re-docking. Although the docking energy does not provide the binding free energy, it reveals structural changes, as reported by Warszycki et al., 2017).

3.4.Structural Analysis

Computational analysis demonstrates that residues, such as Asn, Trp and Pro, induce clustering and stabilize the TM domains of GPCRs (Hanlon & Andrew, 2015; Venkatakrishnan et al., 2013). The overall movement of TM helices during receptor activation is followed by a range of common local microswitches. These microswitches are rotamer shifts occurring in extremely conserved side chains of GPCRs (Nygaard, Frimurer, Holst, Rosenkilde, & Schwartz, 2009). Rotamer shifts depend on whether the residues are facing the lipid bilayer or the protein backbone (Chamberlain & Bowie, 2004). Major helical rearrangements are seen in the CB1 receptor upon receptor activation. TM1 and 2 are compressed, whereas the TM6 shifts its orientation providing room for the ligand to bind (**Figure 3.3**). The microswitches responsible for these shifts are shown in Figure 3.1.

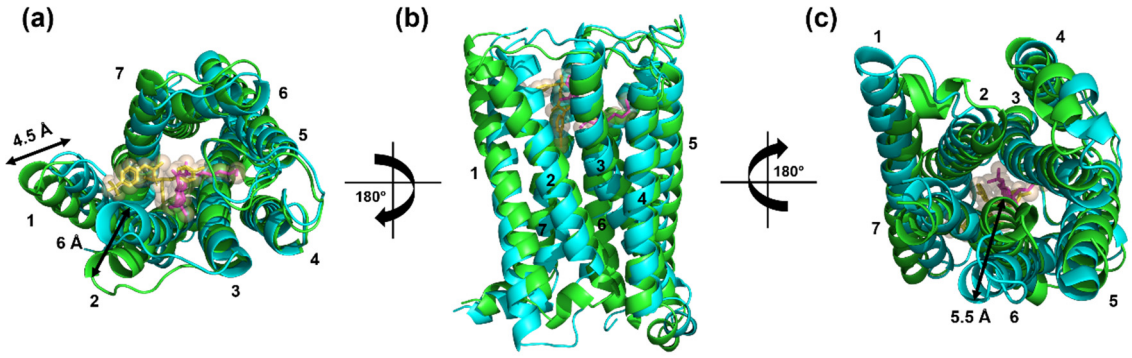

Figure 3.3 Comparison of inactive and active CB1 receptor structures. (**a**) Extracellular view of the inactive (green) structure (PDB ID: 5U09) with the ligand taranabant (yellow; in stick representation) compared with the active (cyan) structure (PDB ID: 5XRA) with the ligand AM11542 (magenta; in stick representation) of the CB1 receptor. (**b**) Side view. (**c**) Cytoplasmic view. The TM domains are labelled in numbers. Significant structural changes are seen upon receptor activation in TM1, 2 and 6. TM1 and 2 are shifted inward by 4.5 Å and 6 Å, respectively, as measured at the α-carbon of Ala 118 and Ile 175 (black arrows) in the two structures respectively. The movement is compensated by TM6 moving outward by 5.5 Å as measured at the α-carbon of Leu 345 (black arrow) in the two structures. (All structural analysis and Figures were made using PyMOL (DeLano, 2002)).

The DRY motif in TM3 is a conserved (upto 96%) region found in class A GPCRs (Katritch, Cherezov, & Stevens, 2013). It has distinct conformation, which facilitates G-protein activation and β-arrestin binding (Gyombolai, Tóth, Tímár, Turu, & Hunyady, 2015). In all the inactive-state GPCR structures, the DRY motif's R214$^{3.50}$ (superscript denotes Ballesteros-Weinstein numbering of GPCR residues) (Ballesteros & Weinstein, 1995) forms a salt bridge with the D213$^{3.49}$ (Vogel et al., 2008). R214$^{3.50}$ forms ionic lock with D338$^{6.30}$. This ionic lock is broken when CB1 changes into the active-state (Shim, Ahn, & Kendall, 2013), resulting in the inward movement of Y397$^{7.53}$ of NPxxY motif and Y294$^{5.58}$ which are the main features of the GPCR active-state (Ballesteros, Shi, & Javitch, 2001, Dror et al., 2011, Fritze et al., 2003). Aromatic stacking between F200$^{3.36}$, W279$^{5.43}$ and W356$^{6.48}$ stabilize the CB1 helical orientation in TM3, TM5 and TM6, respectively (Shim & Padgett, 2013). T210$^{3.46}$ stabilizes R214$^{3.50}$ by forming an extensive water-mediated hydrogen-bonding network with S152$^{2.39}$, D213$^{3.49}$, R214$^{3.50}$, and Y294$^{5.58}$ (Shim, Ahn, & Kendall, 2013).

Y397$^{7.53}$ located in TM7 (92% conserved), acts as an important receptor activation switch in GPCRs. In inactive-state GPCR structures, Y397$^{7.53}$ faces towards TM1 and TM2, whereas in the active-state, rotamer shift is observed in the direction of TM3 and TM6 (Katritch, Cherezov, & Stevens, 2013). This inward movement aids in forming the network of water-mediated hydrogen-bonds with (S/N)LAxAD and NPxxY motifs present in TM2 and TM7 of the CB1 receptor (Shim, Ahn, & Kendall, 2013). The large outer dislocation of TM6 and inner movement of TM7 provide the mechanism for GPCR activation upon agonist binding (Mallipeddi, Janero, Zvonok, & Makriyannis, 2017). In the CB1-G_i model, D163$^{2.50}$ of (S/N)LAxAD motif and N393$^{7.49}$ form a water channel (Shim, Ahn, & Kendall, 2013), as an indication for stabilizing the active state in GPCRs (Grossfield, Pitman, Feller, Soubias, & Gawrisch, 2008). D163$^{2.50}$ forms direct H-bonds with S203$^{3.39}$ and S390$^{7.46}$, N393$^{7.49}$ of the NPxxY motif and a water-mediated H-bond to N134$^{1.50}$. This H-bond network is extended by N393$^{7.49}$ forming water-mediated H-bonds with N389$^{7.45}$ and Y397$^{7.53}$ (Shim & Padgett, 2013). Aromatic stacking is observed between W356$^{6.48}$ and W279$^{5.43}$ which is essential for the CB1 receptor activation through the rigid motion of TM6 (Shim et al., 2011). The location of these motifs, also known as microswitches or switches, are shown in Figure 3.1 and additional details are available from Hauser et al. (Hauser et al., 2018).

3.5.CB1 variant analysis

Since GPCR signaling involves an elaborate conformational change, including the breaking of the ionic lock, we then proceeded with detailed structural analysis to understand the basis of the observed experimental effects. D163$^{2.50}$ of (S/N)LAxAD motif is a conserved residue in GPCRs. It is crucial for stabilizing the active receptor conformation. From our analysis, the D163E and D163N mutants altered the TM2 orientation towards TM7. The D163E mutant in the inactive state has two polar contacts with N134 and S390. Similarly the D163E and D163N mutants in active state show two polar contacts with S203 and S390. These contacts draw TM3 and TM7 closer to TM2, decreasing the space available for ligands to bind. Conversely, the D163Y mutation, which does not have any experimental data, is found to stabilize the receptor, as tyrosine extends two strong polar contacts with S203 in TM3 and N389 in TM7, in both the inactive and active conformations, without affecting the ligand binding site. These new interactions indirectly help in stabilizing the helices, making them favourable for ligand binding (**Figure 3.4**). Overall, D163N shows distinct differences between the inactive and active structures, which could be explored further by MD simulations.

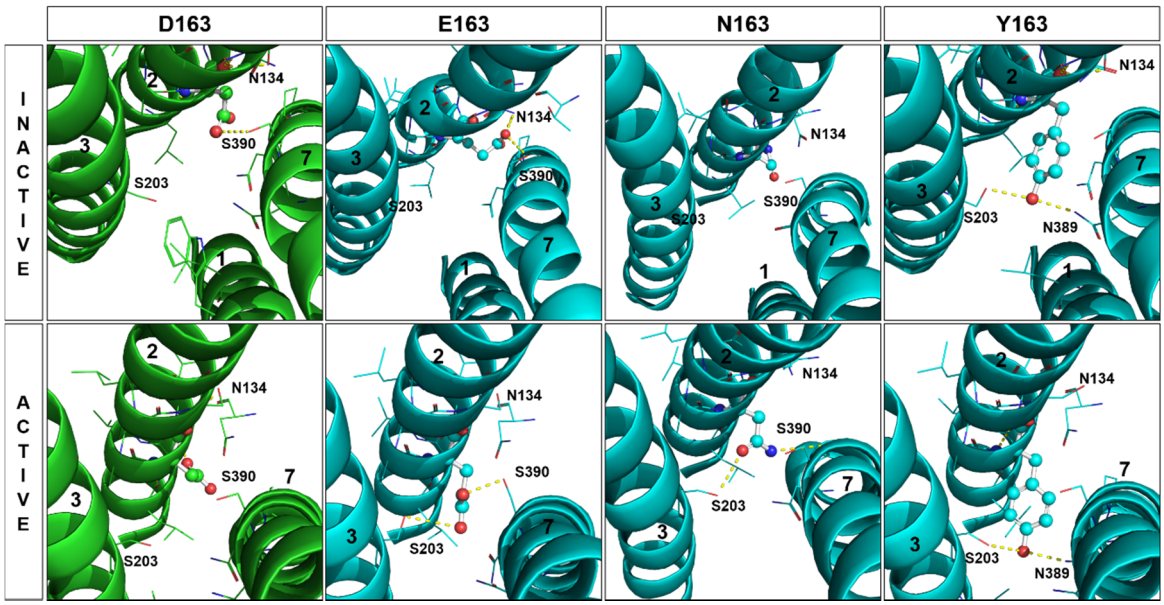

Figure 3.4 CB1 D163 variants. Comparison of interactions in the inactive (PDB ID: 5U09) and active (PDB ID: 5XRA) CB1 receptor structures are shown.

Mutation in the K192$^{3.28}$ resulted in indirect modification of the ligand binding pocket geometry, as K192$^{3.28}$ forms a hydrogen bond with the OH group of S173 with most of the cannabinoid ligands bound (Shim, 2010). In the inactive state, the K192E mutant receptor loses its strong interaction with the residues, D176 and D184, present in the EC2 loop (**Figure 3.5** (**a**)). In both the inactive and active states, E192 readily forms a hydrogen bond with S173 from TM2. This substitution of negatively charged residue leads to structural perturbation, especially since the EC2 loop residues are no longer tethered. As K192 is close to the DRY motif, involved in switching and receptor activation, this mutation needs to be explored further by MD simulations.

An intra-loop disulfide bond is present in CB1 receptor in the EC2 loop between C264 and C257, which is important for ligand recognition, receptor activation and stability. Changes to these cysteines, as observed independently in the C257A and C264A mutants, causes the disulfide bond to break, losing the interactions with residues Q261 and S262, which are important for ligand internalization (**Figure 3.5**(**b**)), Thus, as a result of either of these mutations, the CB1 receptor functionality will be totally affected, which is in accord with the results of experimental assays (Fay et al., 2005).

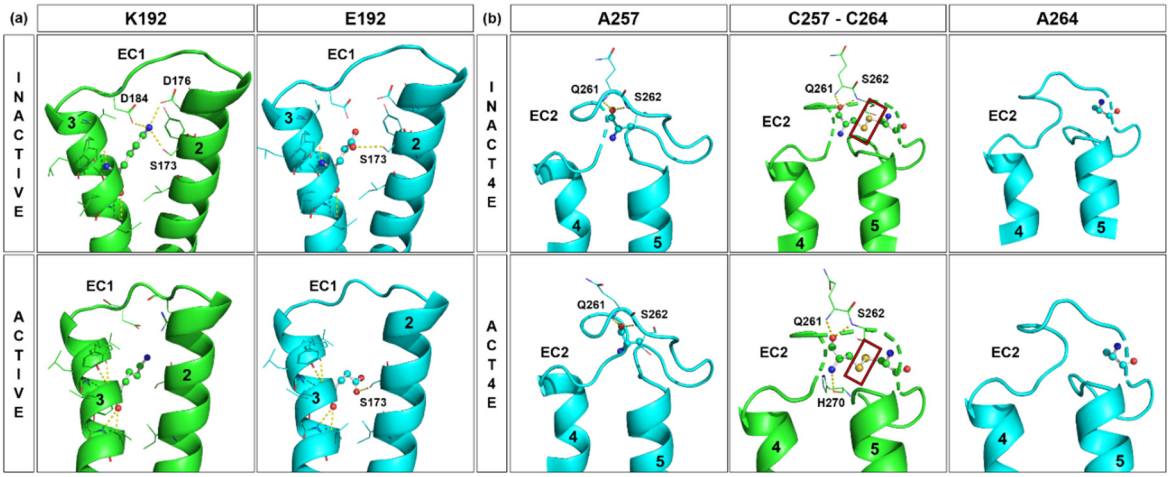

Figure 3.5 CB1 variants at positions 192, 257 and 264. (**a**) K192E variant interaction comparison in the inactive (PDB ID: 5U09) and active (PDB ID: 5XRA) CB1 receptor structures. (**b**) C257A and C264A variant interaction comparison in the inactive (PDB ID: 5U09) and active (PDB ID: 5XRA) CB1 receptor structures.

The aromatic cluster in TM 4 and TM 5 are crucial for ligand binding. The Y275F mutant loses its hydrogen bond with I247 in TM 4 in both the inactive- and active-state conformations (**Figure 3.6**(**a**)). The experimental consequence of this mutation is decreased ligand affinity (McAllister et al., 2002), leading to cAMP inhibition. In spite of aromatic substitution, even slight changes in the orientation of the aromatic residue may affect ligand retention as well as maintaining the receptor in active-state.

W299 is the last residue in TM 5. The W299R mutant fails to interact with the IC3 loop. The W299R mutant side chain is located in the aqueous domain on the intracellular side of the membrane and is not involved in interactions with the IC3 loop (**Figure 3.6**(**b**)) in the active and inactive structures. From our results, this mutant is unlikely have any functional consequences.

R336 and R340 in the IC3 of CB1 interact closely with $G\alpha_i$ domain of the G-protein during signal transduction (Shim, Ahn, & Kendall, 2013). In the R336C mutant receptor, the interaction with the neighboring residues in the IC3 loop is lost (**Figure 3.7**(**a**)). Under this circumstance, signal internalization may be affected. Further analysis is required to fully understand the consequence of the R336C mutation, when the structure of IC3 becomes available, with the bound G-protein.

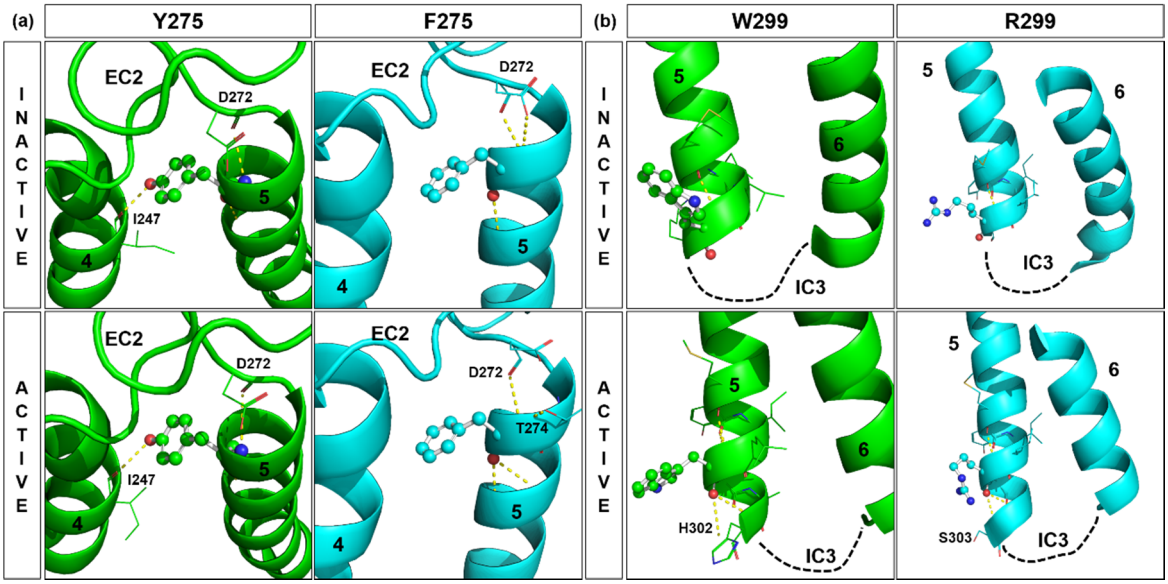

Figure 3.6 CB1 variants at positions 275 and 299. (**a**) Y275F variant interaction comparison in the inactive (PDB ID: 5U09) and active (PDB ID: 5XRA) CB1 receptor structures. (**b**) W299R variant interaction comparison in the inactive (PDB ID: 5U09) and active (PDB ID: 5XRA) CB1 receptor structures.

C355$^{6.47}$ of the CWxP motif is critical in binding classical cannabinoids, which encourage receptor internalization *via* β-arrestin-mediated pathways (Gyombolai, Tóth, Tímár, Turu, & Hunyady, 2015). A helical kink is seen in TM 6 at C355, which is important in the active conformation. As a result of C355A mutation, it is found there is no significant change in the helical orientation (**Figure 3.7**(**b**)). C355$^{6.47}$ is a direct contact residue for binding the synthetic cannabinoid, CP55940. The C355A mutant retained the binding affinity for CP55940 (Shim, 2010), which supports our analysis.

The M363A variant did not show any structural change (**Figure 3.8**(**a**)). As M363 is implicated in binding the synthetic cannabinoid, HU-210, with the M363A variant showing a slight decreased in ligand binding affinity towards HU-210 (Shim et al., 2011). Further analysis by molecular dynamics simulation could reveal the changes due to mutation.

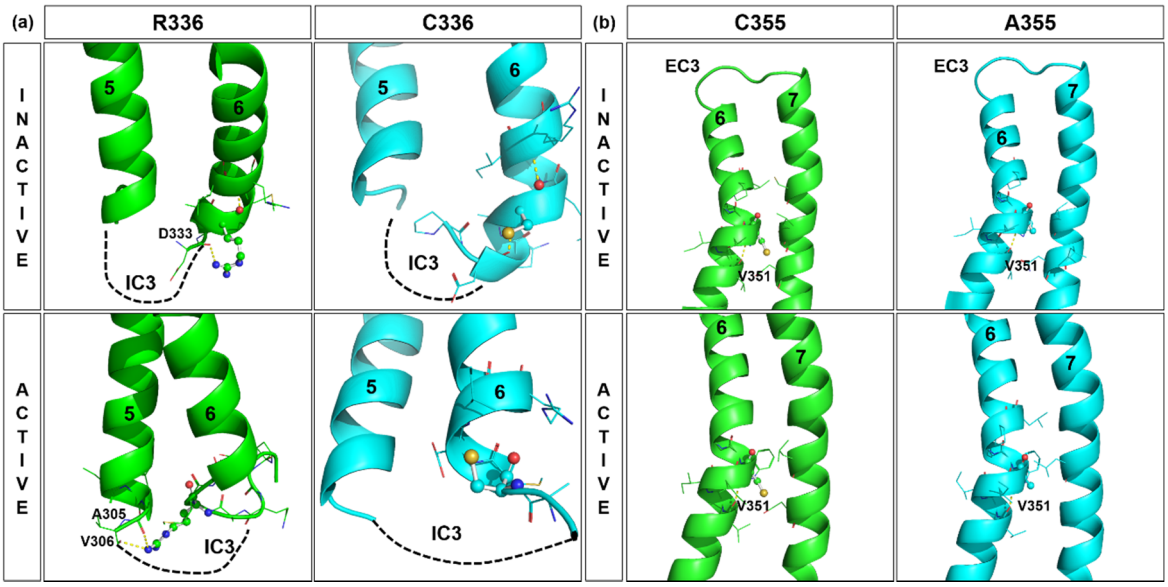

Figure 3.7 CB1 variants at positions 336 and 355. (**a**) R336C variant interaction comparison in the inactive (PDB ID: 5U09) and active (PDB ID: 5XRA) CB1 receptor structures. (**b**) C355A variant interaction comparison in the inactive (PDB ID: 5U09) and active (PDB ID: 5XRA) CB1 receptor structures. Dotted lines show the part of the modelled IC3 loop which is missing in the experimental structures.

Y397$^{7.53}$ along with Y294$^{5.58}$ contribute to the breakage of the ionic lock for receptor activation. TM 2 and 7 are closer in the active-state wild type receptor, compared to the inactive-state structure. In the Y397C mutant, TM 2 and TM 7 are further away (**Figure 3.8**(**b**)) possibly delaying the ionic lock breakage and affecting receptor activation (Shim, 2010). Further analysis by molecular dynamics simulations would provide greater detail of the functional consequences of this mutation.

In summary, structural bioinformatics analysis results were in accord with reported experimental studies for seven of the eight variants (excluding M363A) and could provide functional consequences for three of the remaining variants (D163Y, W299R and Y397C). R336C needs to further investigation when the structure of the intact IC3 is available.

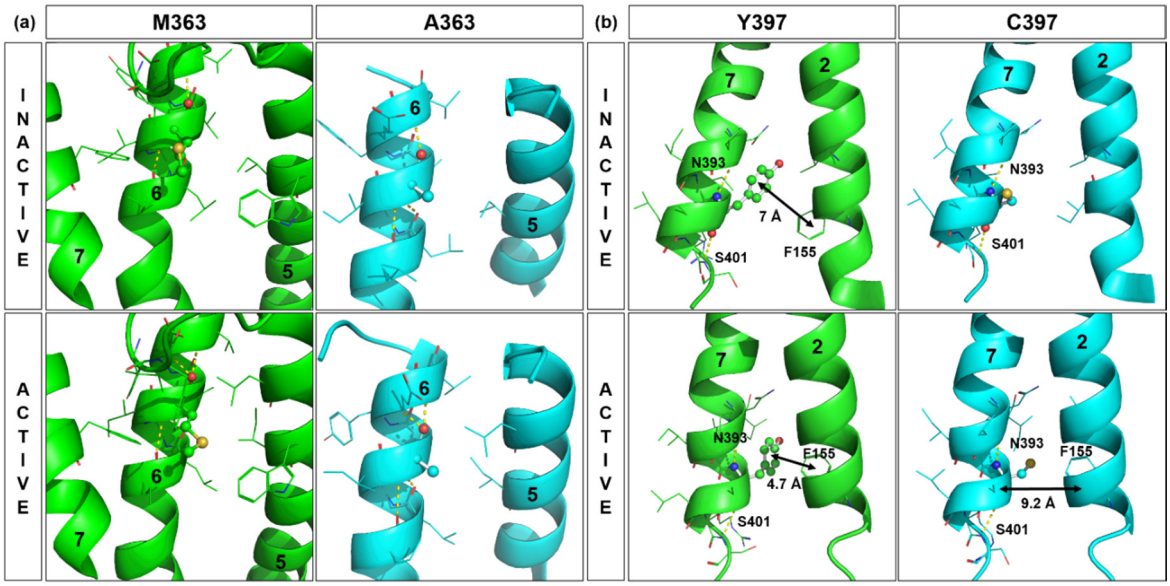

Figure 3.8 CB1 variants at positions 363 and 397. (**a**) M363A variant interaction comparison in the inactive (PDB ID: 5U09) and active (PDB ID: 5XRA) CB1 receptor structures. (**b**) Y397C variant interaction comparison in the inactive (PDB ID: 5U09) and active (PDB ID: 5XRA) CB1 receptor structures.

3.6.Molecular Dynamics

Based on the structural analysis carried out, four mutations, D163N, K192E, M363A and Y397C in the TM regions, were selected for MD simulations. Jung at el., (Jung, Cho, & Yu, 2018) have reported a similar study with the partial agonist, THC; an antagonist, THCV (the propyl analogue of THC) and the inverse agonist, taranabant. However, the endocannabinoid anandamide would be most useful in understanding the physiological consequences of CB1 mutations. The docked structures with anandamide described above were chosen as the starting point of 100ns (1µs) MD simulations. A total of ten structures were used for the simulations: wild and four variants of CB1 in both the inactive- and active-state conformations. Backbone RMSD was calculated for all the systems from the simulated structures. It was considered as an average measure for the convergence of the system.

A total of ten structures were used for the simulations: wild and four variants of complex CB1 structures in both the inactive- and active-state conformations. The modelled structures docked with the endogenous ligand anandamide were used for simulation.

From the RMSD values, we observed considerable structural deviation in the variant structures compared to the wild type structure. The wild type inactive-state structure showed a high standard deviation in the range (~3Å to ~6Å) when compared to the active-state

structure (~3Å to ~5Å). During the course of the simulation, all the variants showed high stability until ~40ns to ~50ns time frame in the inactive-state. Whereas in the active-state, the structural stability was reached beyond ~30ns to ~40ns, with an exception of the Y397C variant which showed abnormal stability when compared to the wild structure throughout the progress of simulation (**Figure 3.9**). This structural stability analysis is in accordance with these substitutions most likely to affect the receptor activation at the initial stage.

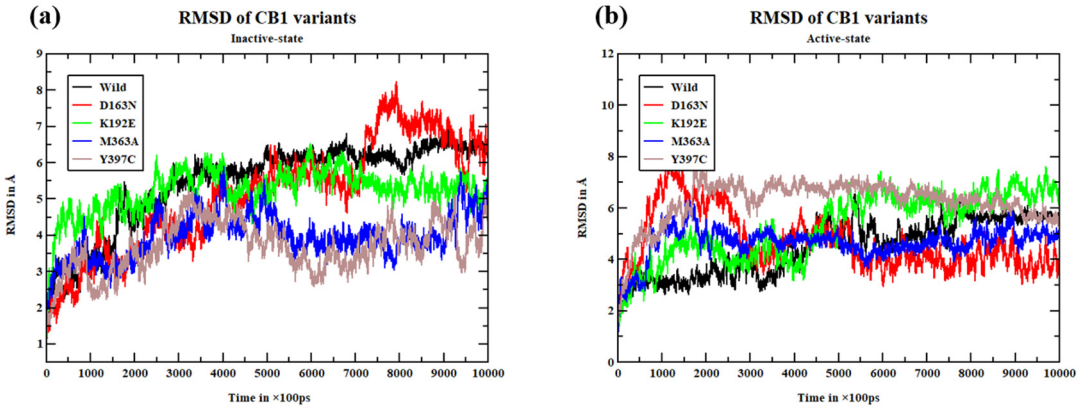

Figure 3.9 RMSD of the wild and mutant structures of the CB1 receptor. (**a**) The inactive-state, (**b**) the active-state RMSD values are shown. The abscissa represents the simulation time in ps, and the ordinate represents the RMSD distance in Å. The black, red, green, blue and brown lines represent the wild type structure and the D163N, K192E, M363A and Y397C variant structures respectively.

This simulation analysis gives an idea of long-range motion and thermal fluctuation of the residues. The variant's structural flexibility was evaluated from the calculated RMSF values. The modelled IC3 loop residues exhibited massive fluctuation in all the simulation system. The D163N, M363A, Y397C variants showed higher fluctuation (~10Å to ~12Å) when compared to the wild and K192E variant structure (~7Å to ~8Å) in the inactive-state conformation. While the active-state conformation the D163N variant and the wild type structures showed similar fluctuations (~1Å to ~3Å), the K192E, M363A and Y397C variant structures presented more fluctuations (~8Å to ~10Å) altogether. (**Figure 3.10**).

Protein structural modification was evaluated from the calculated Radius of gyration values. RoG gives an overview of the protein conformation in its actual oriented state throughout the course of the simulation. This analysis suggested the Radius of gyration for the variants were comparatively increased with the wild structure in both the inactive- and active-state conformations. This indicates these substitutions increase the structural

flexibility and relaxing the protein structure thereby altering and losing the protein conformation and the geometry respectively. The D163N, K192E and Y397C variants exhibited high flexibility in the inactive-state, while in the active-state all the variants showed were only slightly more flexible than the respective wild type protein structure. (**Figure 3.11**).

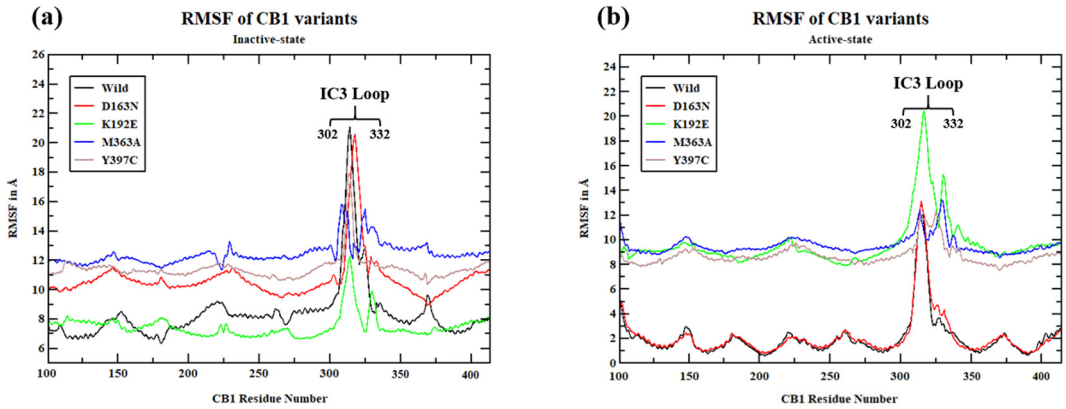

Figure 3.10 RMSF of the wild and mutant structures of the CB1 receptor. (**a**) The inactive-state and (**b**) the active-state RMSF values are shown. The abscissa represents the CB1 residues number, and the ordinate represents the RMSF distance in Å. The black, red, green, blue and brown lines represent the Wild, D163N, K192E, M363A and Y397C variant structures respectively.

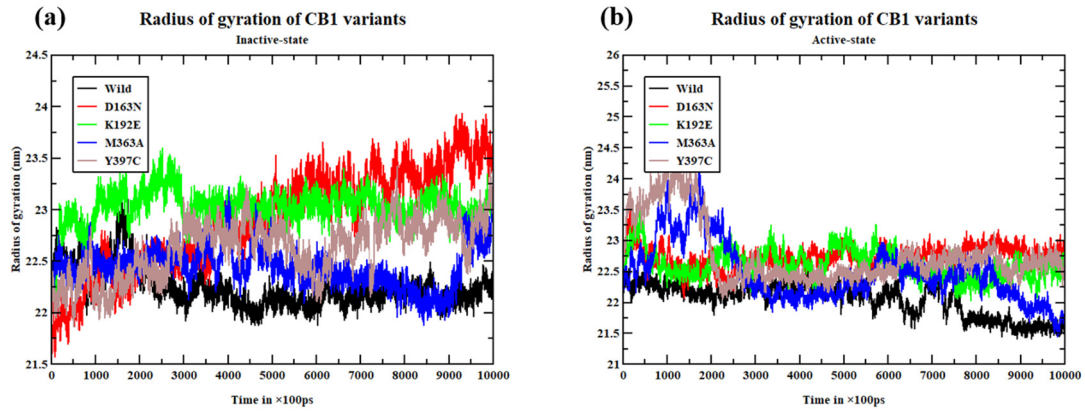

Figure 3.11 The radius of gyration of the wild and mutant structures of the CB1 receptor. (**a**) The inactive-state and (**b**) the active-state radius of gyration values are shown. The abscissa represents the simulation time in ps, and the ordinate represents the radius of gyration distance in Å. The black, red, green, blue and brown lines represent the Wild, D163N, K192E, M363A and Y397C variant structures respectively.

Hydrogen bonds are the primary connections for upholding the stability of the protein structure. Estimating the number of intramolecular hydrogen bonds formed during the simulation is essential to judge the stability of the protein structure. The wild structures in the inactive- and active-state formed an average of ~130 to ~150 hydrogen bonds. Notably, the number of hydrogen bonds in the variant structures are varied. The D163N, K192E and M363A variants formed a number of hydrogen bonds ~150 to ~180 in both the conformations. But in the Y397C variant, the total hydrogen bonds formed are more or less equal with the wild structure (**Figure. 3.12**).

This remarkable change in the number of hydrogen bonds reflects the impact of substitutions and disrupt the local protein environment. Such loss or gain of hydrogen bonds can alter the interactions near the substitution and change the residue-solvent interaction and charge distribution.

The SASA of the CB1 variants was calculated in both the inactive- and active-state conformations. From the analysis, the wild type structure showed a SASA of ~18000 to ~18500 $Å^2$ in the inactive-state. In the active-state, the CB1 receptor had a SASA of ~18500 to ~19000 $Å^2$. However, the variant structures captured more surface area. The D163N, K192E and M363A variants had little more area ~500 $Å^2$ than the wild type structure in both the conformations. The Y397C variant also showed the same change in the inactive-state, but in the active-state conformation, it netted ~19000 to ~20500 $Å^2$ of surface area (**Figure 3.12**). This observation specifies that repositioning of buried hydrophobic residues as an effect of substitutions causes a change in solvation energy of the protein. The analysis suggests that the substitutions have relaxed the protein conformation yielding more surface area. Thereby disturbing the ligand binding tendencies.

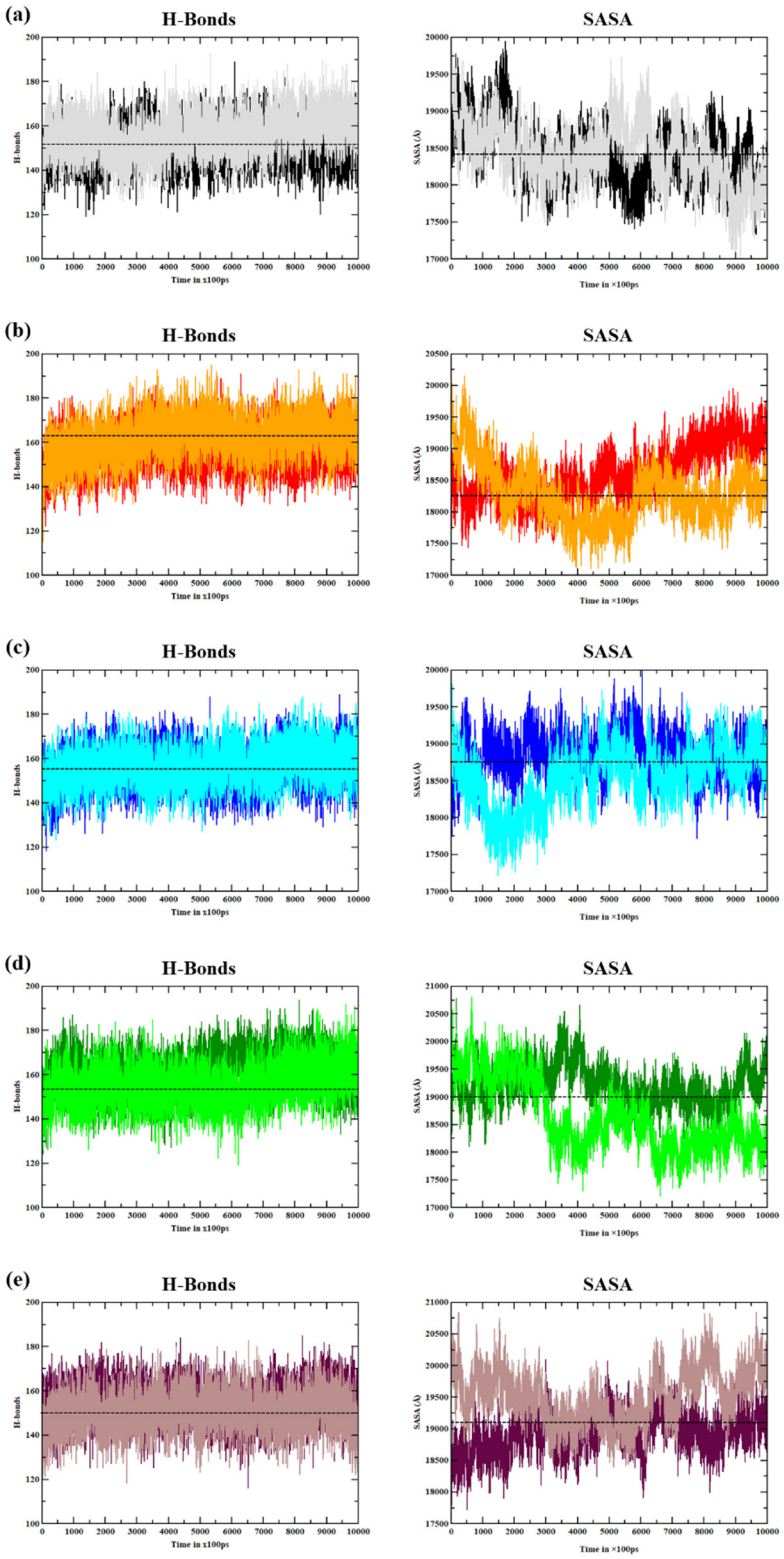

Figure 3.12 Hydrogen bonds and SASA comparison in the CB1 receptor. The number of hydrogen bonds and SASA values (y-axis) are shown for (**a**) WT, (**b**) D163N, (**c**) K192E, (**d**) M363A and, (**e**) Y397C, as a function of the simulation time in ps (x-axis). The black, red, blue, green and maroon colors represents the inactive-state, whereas the grey, orange, cyan, light green and brown colors represents the active-state of the receptor. The dotted line is the position of the overall wild type mean value.

Finally, the binding free energy decomposition of CB1-ligand complexes was calculated, by extracting the 100 snapshots from the last 5ns trajectory of each MD simulation, using the MMPBSA (Molecular Mechanics Poisson-Boltzmann surface area) approach (Gohlke, & Case, 2004). The binding free energy of each complex was calculated by the following equation.

$$\Delta G_{bind} = G_{complex} - (G_{protein} + G_{ligand})$$

Table 3.2. **Binding energy calculated by MMPBSA method**. Calculated binding free energy for the different CB1-ligand complexes using MMPBSA method, in the active and inactive conformations.

ΔG (kcal/mole) values obtained from MMPBSA

Ligand	**CB1 structure**	**CB1 conformation**	
		Inactive	**Active**
Anandamide	WT	-15.3026	-22.5762
	D163N	-20.657	-11.9748*
	K192E	-6.95*	-17.7868
	M363A	-14.1487	-19.786
	Y397C	-5.9101*	-8.3001*

*significant

Binding free energy for anandamide with the native and four mutant structures in the active and inactive states are shown in Table 2. As the data is sparse, we computed the fold change between the mutant and WT ΔG values and statistically significant values (>log2(1.5)=0.585) are marked with an asterisk in **Table 3.2**. Notably, D163N weakens ligand binding to the active CB1 receptor structure (log2FC = 0.915), while K192E has a similar effect on the inactive CB1 structure (log2FC=1.139). Y397C severely decreases ligand binding to both the active (log2FC=1.444) and the inactive (log2FC=1.373) structures. M363A did not affect ligand binding seriously, as noted earlier from docking and structural analysis, perhaps because anandamide is much smaller than the agonist HU-210 (Shim, 2010).

4. Discussion

In the past decade, there were many advances in membrane protein engineering, heterologous protein expression, site-directed mutagenesis for receptor stabilization, and crystallization techniques with different lipid cubic phase (LCP) methods incorporating micelles, bicelles and nanodiscs (Xiang et al., 2016). The first GPCR X-ray crystal structure to be solved is the bovine rhodopsin (PDB ID: 1F88) (Palczewski et al., 2000). Later in 2007, the most widely characterized GPCR, the human β_2-adrenergic receptor (β_2AR) (PDB ID: 2RH1) (Cherezov et al., 2007) crystal structure was determined. GPCR structure elucidation has encountered a rapid growth and continuing to be a challenging task. To date, 271 structures of 53 distinct receptors (including four species orthologues) are listed in GPCRdb (http://gpcrdb.org/) (Munk et al., 2019), covering four major GPCR classes: A, B1 (Secretin), C (Glutamate) and F (Frizzled). However, 87% of GPCRS completely lack structural information, including all members classes B2 (Adhesin) and T (Taste 2). The ActiveGEnSeMBLE computational scheme identifies the active conformations in GPCRs, facilitating targeted GPCR drug designing (Dong, Goddard, & Abrol, 2017). Similar to CB1 structures, GPCR structures lack the highly variable regions such as the extracellular and the intracellular loops which need to be modelled *in silico* for structural studies. Generally, these flexible regions are not solved in the crystal structure and substituted by a fused protein, such as lysozyme (Moreira, 2014). For GPCRs with no structural information, structural models are a first step towards understanding functional consequences of variants and for variant-specific ligand design, followed by molecular docking and molecular dynamics simulations. To this end, the GPCR-SSFE (Sequence-Structure-Feature-Extractor) (Worth, Kreuchwig, Kleinau, & Krause, 2011) and the GPCR-ModSim (Esguerra, Siretskiy, Bello, Sallander, & Gutiérrez-de-Terán, 2016) provides homology models of GPCRs, which can be utilized for studies of GPCRs without experimental structures. GPCR-ModSim incorporates the best-known homology modelling program, MODELLER version 9.20 (Web & Sali, 2016) MemProtMD is a database of membrane proteins embedded in the lipid bilayer (Newport, Sansom, & Stansfeld, 2019), allowing structure-based drug discovery, based on Coarse-Grained Self-Assembly simulations. The GPCR NaVa (Natural Variants) database provides information about human GPCR variants, which can be considered during variant-specific drug development (Kazius et al., 2008) , based on primary data derived from GPCRdb (Pándy-Szekeres et al., 2018). The Sensor-based GPCR ligand screening is an alternative strategy for structure-based ligand screening approach, which identifies novel allosteric ligands (Kumari, Ghosh, & Shukla, 2015). The Google's Exacycle a cloud-based computing

platform can be used for increased timescale molecular dynamics simulations of GPCRs (Kohlhoff et al., 2014). All these computational resources will be extremely useful for drug development for GPCRs without any structural information.

The activation mechanism of rhodopsin receptor (Smith, 2012), β_2AR (Dror et al., 2011), and μ-opioid receptor (Huang et al., 2015) are well characterized. Such structural information will give an idea to understand other GPCRs, whose activation mechanism is not studied. Additionally, GPCRs structural information can also provide the molecular basis of ligand recognition and delineate the concept of GPCRs mechanism. For instance, the CB1-G_i complex model describes the key contacts residues contributing to CB1 activation (Shim, Ahn, & Kendall, 2013). Similarly, the recently available CB1-G_i protein complex structure (Krishna Kumar et al., 2019) describes how the MDMB-Fubinaca locks the receptor in the active-state through the toggle switch residues $F200^{3.36}$/$W356^{6.48}$.

The GPCR SNPs are widely characterized, the β_2AR SNPs are computationally characterized and analysing the variant β_2AR receptor dynamics discloses the variant's effect on receptor function (Sengupta, Sonar, & Joshi, 2017; Tandale, Joshi, & Sengupta, 2016). However, the CB1 SNPs are not examined in detail up to now. But, the CB1 ligand efficiency has been studied by computational methods, including molecular docking and molecular dynamics simulation. Ligand binding preferences for different conformations of the CB1 receptor has also been studied (Jung, Cho, & Yu, 2018). To supplement these studies, this initial mapping of SNPs on CB1 receptor structure, followed by the variant receptor structural analysis had shed some lime light on the mutational effects of CB1. Comparative structural analysis can give genotypic-phenotypic correlation (Huynh, Khan, & Ranganathan, 2011). as and when new GPCR structures become available. To extent this report, further studies could use servers such as DynaMut can be used to assess the impact of mutation on the protein structure and function (Rodrigues, Pires, & Ascher, 2018). The sequence-function relationships map with integrative models of protein evolution can help to identify mutations that are likely to GPCR function reliably (Studer, Dessailly, & Orengo, 2013).

The mutational effects on GPCRs for designing high potency drugs, to combat with GPCR associated disease conditions, remains a challenge. Correspondingly, *in vitro* polymorphism studies on the human μ-opioid receptor gene revealed the decreased signalling of morphine and other endogenous opioids which contributes to substance abuse (Knapman & Connor, 2015; Knapman, Santiago, & Connor, 2015). High level of anandamide concentration in a patient's body had shown pain insensitivity due to a

microdeletion in FAAH pseudogene (Habib et al., 2019). Hardianto et al. (Hardianto, Khanna, Liu, & Ranganathan, 2019) have shown, the different dynamic features of a protein can be determined by molecular dynamics approach. Similarly, five basic parameters (RMSD, RMSF, Radius of gyration, Hydrogen bonds and SASA) were analyzed in the different CB1 receptor conformation with its endogenous ligand anandamide through 100ns of molecular dynamics simulation. Molecular stability was assessed through RMSD. Whereas protein stability was analyzed through RMS fluctuation. The conformational changes, protein rigidity and flexibility are required for a protein to function normally. Such deviation and enhanced flexibility as observed in the CB1 variant structure can adversely affect the CB1 receptor function. The higher flexibility exhibited by the variant structures analyzed by measuring the radius of gyration distance, as well as calculating the increased or decreased number of hydrogen bonds formed, infers how the substitutions can perturb the protein function. In order to measure the space available for the solvent to interact with the protein was estimation by SASA. Such analysis will help us to know the hydrophobic nature of the protein exterior while designing small potent ligand molecules. Overall from the molecular dynamics simulation analysis, it is clear that the CB1 receptor is very much influenced by the SNPs. Especially the Y397C variant does not coincide with the wild structure. As Y397 contributes in the breakage of ionic lock for CB1 receptor activation. This aromatic substitution can change the receptor activation mechanism. Hence it is crucial to do the further experimental evaluation in combatting the substitution effect on the CB1 receptor. Early structural insight on the CB1 receptor can lay a foundation for further experimental analysis of polymorphisms and can help us to understand better about the receptor conformation and ligand binding tendencies and finally to design the best ligand to treat all the cannabinoid disorder.

5. Conclusions

I have briefly examined the functional consequences of variants on GPCRs, as reported in recent literature. For the cannabinoid receptor 1, the availability of inactive and active ligand-bound experimental structures provided an opportunity to carry out detailed structural bioinformatics analysis of mutant structures as well as explore the mutational effect on ligand binding using two agonists, an inverse agonist and an antagonist. Structural bioinformatics analysis confirmed the experimental observations for the several variants, providing the opportunity to extend this approach to SNPs that did not have any reported experimental observations. Analysis of MD simulations confirmed the deleterious nature of D163N, K192E and Y397C and helped in understanding experimental results for M363A.

This study can be extended in the future, by carrying out structural mapping of all the 38 mutants immediately below the cutoff threshold, followed by extensive MD simulations with different ligands. Such an approach will assist in designing phenotype-specific drugs, as described by Hauser et al. (Hauser et al., 2018).

References

Ahmed, S. A., Ross, S. A., Slade, D., Radwan, M. M., Zulfiqar, F., & ElSohly, M. A. (2008). Cannabinoid Ester Constituents from High-Potency Cannabis sativa. *Journal of Natural Products*, *71*(4), 536–542.

Allen, M. P. (2004). Introduction to molecular dynamics simulation. *Computational Soft Matter: From Synthetic Polymers to Proteins*, *23*, 1–28.

Atakan, Z. (2012). Cannabis, a complex plant: different compounds and different effects on individuals. *Therapeutic Advances in Psychopharmacology*, *2*(6), 241–254.

Atwood, B. K., & Mackie, K. (2010). CB2: a cannabinoid receptor with an identity crisis. *British Journal of Pharmacology*, *160*(3), 467–479.

Baker, E. N., & Hubbard, R. E. (1984). Hydrogen bonding in globular proteins. *Progress in Biophysics and Molecular Biology*, *44*(2), 97–179.

Ballesteros, J. A., & Weinstein, H. (1995). Integrated methods for the construction of three-dimensional models and computational probing of structure-function relations in G protein-coupled receptors. In S. C. Sealfon (Ed.), *Methods in Neurosciences*, pp. 366–428.

Ballesteros, J. A., Shi, L., & Javitch, J. A. (2001). Structural mimicry in G protein-coupled receptors: implications of the high-resolution structure of rhodopsin for structure-function analysis of rhodopsin-like receptors. *Molecular Pharmacology*, *60*(1), 1–19.

Baye, T. M., Zhang, Y., Smith, E., Hillard, C. J., Gunnell, J., Myklebust, J., … Wilke, R. A. (2008). Genetic variation in cannabinoid receptor 1 (CNR1) is associated with derangements in lipid homeostasis, independent of body mass index. *Pharmacogenomics*, *9*(11), 1647–1656.

Bendl, J., Stourac, J., Salanda, O., Pavelka, A., Wieben, E. D., Zendulka, J., … Damborsky, J. (2014). PredictSNP: Robust and Accurate Consensus Classifier for Prediction of Disease-Related Mutations. *PLoS Computational Biology*, *10*(1).

Benzinou, M., Chèvre, J.-C., Ward, K. J., Lecoeur, C., Dina, C., Lobbens, S., … Froguel, P. (2008). Endocannabinoid receptor 1 gene variations increase risk for obesity and modulate body mass index in European populations. *Human Molecular Genetics*, *17*(13), 1916–1921.

Berg, J. M., Tymoczko, J. L., Gatto, G. J., Stryer, L. (2015). *Biochemistry* (8th ed.). Palgrave Macmillan.

Berman, H. M., Westbrook, J., Feng, Z., Gilliland, G., Bhat, T. N., Weissig, H., … Bourne, P. E. (2000). The Protein Data Bank. *Nucleic Acids Research*, *28*(1), 235–242.

Bidwell, L. C., Metrik, J., McGeary, J., Palmer, R. H. C., Francazio, S., & Knopik, V. S. (2013). Impulsivity, variation in the cannabinoid receptor (CNR1) and fatty acid amide hydrolase (FAAH) genes, and marijuana-related problems. *Journal of Studies on Alcohol and Drugs*, *74*(6), 867–878.

Busquets Garcia, A., Soria-Gomez, E., Bellocchio, L., & Marsicano, G. (2016). Cannabinoid receptor type-1: breaking the dogmas. *F1000Research*, *5*.

Capriotti, E., Altman, R. B., & Bromberg, Y. (2013). Collective judgment predicts disease-associated single nucleotide variants. *BMC Genomics*, *14 Suppl 3*, S2.

Case, D. A., Cheatham, T. E., Darden, T., Gohlke, H., Luo, R., Merz, K. M., … Woods, R. J. (2005). The Amber biomolecular simulation programs. *Journal of Computational Chemistry*, *26*(16), 1668–1688.

Chakrabarti, B., Kent, L., Suckling, J., Bullmore, E., & Baron-Cohen, S. (2006). Variations in the human cannabinoid receptor (CNR1) gene modulate striatal responses to happy faces. *The European Journal of Neuroscience*, *23*(7), 1944–1948.

Chamberlain, A. K., & Bowie, J. U. (2004). Analysis of Side-Chain Rotamers in Transmembrane Proteins. *Biophysical Journal*, *87*(5), 3460–3469.

Cherezov, V., Rosenbaum, D. M., Hanson, M. A., Rasmussen, S. G. F., Thian, F. S., Kobilka, T. S., … Stevens, R. C. (2007). High Resolution Crystal Structure of an Engineered Human β2-Adrenergic G protein-Coupled Receptor. *Science (New York, N.Y.)*, *318*(5854), 1258–1265.

Chin, C. N., Lucas-Lenard, J., Abadji, V., & Kendall, D. A. (1998). Ligand binding and modulation of cyclic AMP levels depend on the chemical nature of residue 192 of the human cannabinoid receptor 1. *Journal of Neurochemistry*, *70*(1), 366–373.

Console-Bram, L., Marcu, J., & Abood, M. E. (2012). Cannabinoid receptors: nomenclature and pharmacological principles. *Progress in Neuro-Psychopharmacology & Biological Psychiatry*, *38*(1), 4–15.

Cornell, W. D., Cieplak, P., Bayly, C. I., Gould, I. R., Merz, K. M., Ferguson, D. M., … Kollman, P. A. (1995). A Second Generation Force Field for the Simulation of Proteins, Nucleic Acids, and Organic Molecules. *Journal of the American Chemical Society*, *117*(19), 5179–5197.

Costa, M., Squassina, A., Congiu, D., Chillotti, C., Niola, P., Galderisi, S., … Del Zompo, M. (2013). Investigation of endocannabinoid system genes suggests association between peroxisome proliferator activator receptor-α gene (PPARA) and schizophrenia. *European Neuropsychopharmacology: The Journal of the European College of Neuropsychopharmacology*, *23*(7), 749–759.

Cravatt, B. F., & Lichtman, A. H. (2004). The endogenous cannabinoid system and its role in nociceptive behavior. *Journal of Neurobiology*, *61*(1), 149–160.

D'Antona, A. M., Ahn, K. H., & Kendall, D. A. (2006). Mutations of CB1 T210 produce active and inactive receptor forms: correlations with ligand affinity, receptor stability, and cellular localization. *Biochemistry*, *45*(17), 5606–5617.

D'Antona, A. M., Ahn, K. H., Wang, L., Mierke, D. F., Lucas-Lenard, J., & Kendall, D. A. (2006). A cannabinoid receptor 1 mutation proximal to the DRY motif results in constitutive activity and reveals intramolecular interactions involved in receptor activation. *Brain Research*, *1108*(1), 1–11.

Daiger, S. P., Sullivan, L. S., & Bowne, S. J. (2013). Genes and mutations causing retinitis pigmentosa. *Clinical Genetics*, *84*(2), 132–141.

Darden, T., York, D., & Pedersen, L. (1993). Particle mesh Ewald: An N·log(N) method for Ewald sums in large systems. *The Journal of Chemical Physics*, *98*(12), 10089–10092.

DeLano, W. (2002). *The PyMOL Molecular Graphics System*. http://www.pymol.org.

den Boon, F. S., Chameau, P., Schaafsma-Zhao, Q., van Aken, W., Bari, M., Oddi, S., … Werkman, T. R. (2012). Excitability of prefrontal cortical pyramidal neurons is modulated by activation of intracellular type-2 cannabinoid receptors. *Proceedings of the National Academy of Sciences of the United States of America*, *109*(9), 3534–3539.

Devane, W. A., Dysarz, F. A., Johnson, M. R., Melvin, L. S., & Howlett, A. C. (1988). Determination and characterization of a cannabinoid receptor in rat brain. *Molecular Pharmacology*, *34*(5), 605–613.

Devane, W., Hanus, L., Breuer, A., Pertwee, R., Stevenson, L., Griffin, G., … Mechoulam, R. (1992). Isolation and structure of a brain constituent that binds to the cannabinoid receptor. *Science*, *258*(5090), 1946–1949.

Dhopeshwarkar, A., & Mackie, K. (2014). CB2 Cannabinoid Receptors as a Therapeutic Target—What Does the Future Hold? *Molecular Pharmacology*, *86*(4), 430–437.

Di Marzo, V., Stella, N., & Zimmer, A. (2015). Endocannabinoid signalling and the deteriorating brain. *Nature Reviews. Neuroscience*, *16*(1), 30–42.

Dickson, C. J., Madej, B. D., Skjevik, Å. A., Betz, R. M., Teigen, K., Gould, I. R., & Walker, R. C. (2014). Lipid14: The Amber Lipid Force Field. *Journal of Chemical Theory and Computation*, *10*(2), 865–879.

Dong, S., Goddard, W. A., & Abrol, R. (2017). Identifying multiple active conformations in the G protein-coupled receptor activation landscape using computational methods. *Methods in Cell Biology*, 111–118.

Dror, R. O., Dirks, R. M., Grossman, J. P., Xu, H., & Shaw, D. E. (2012). Biomolecular simulation: a computational microscope for molecular biology. *Annual Review of Biophysics*, *41*, 429–452.

Dror, R. O., Pan, A. C., Arlow, D. H., Borhani, D. W., Maragakis, P., Shan, Y., … Shaw, D. E. (2011). Pathway and mechanism of drug binding to G-protein-coupled receptors. *Proceedings of the National Academy of Sciences of the United States of America*, *108*(32), 13118–13123.

Egertová, M., & Elphick, M. R. (2000). Localisation of cannabinoid receptors in the rat brain using antibodies to the intracellular C-terminal tail of CB. *The Journal of Comparative Neurology*, *422*(2), 159–171.

Eisenberg, D., & McLachlan, A. D. (1986). Solvation energy in protein folding and binding. *Nature*, *319*(6050), 199.

Eissenstat, M. A., Bell, M. R., D'Ambra, T. E., Alexander, E. J., Daum, S. J., Ackerman, J. H., … Olefirowicz, E. M. (1995). Aminoalkylindoles: structure-activity relationships of novel cannabinoid mimetics. *Journal of Medicinal Chemistry*, *38*(16), 3094–3105.

Elsohly, M. A., & Slade, D. (2005). Chemical constituents of marijuana: The complex mixture of natural cannabinoids. *Life Sciences*, *78*(5), 539–548.

Esguerra, M., Siretskiy, A., Bello, X., Sallander, J., & Gutiérrez-de-Terán, H. (2016). GPCR-ModSim: A comprehensive web based solution for modeling G-protein coupled receptors. *Nucleic Acids Research*, *44*(W1), W455-462.

Fay, J. F., Dunham, T. D., & Farrens, D. L. (2005). Cysteine residues in the human cannabinoid receptor: only C257 and C264 are required for a functional receptor, and steric bulk at C386 impairs antagonist SR141716A binding. *Biochemistry*, *44*(24), 8757–8769.

Fernández-Ruiz, J., Romero, J., & Ramos, J. A. (2015). Endocannabinoids and Neurodegenerative Disorders: Parkinson's Disease, Huntington's Chorea, Alzheimer's Disease, and Others. *Handbook of Experimental Pharmacology*, *231*, 233–259.

Ferrara, P., Apostolakis, J., & Caflisch, A. (2002). Evaluation of a fast implicit solvent model for molecular dynamics simulations. *Proteins*, *46*(1), 24–33.

Fredriksson, R., Lagerström, M. C., Lundin, L.-G., & Schiöth, H. B. (2003). The G-protein-coupled receptors in the human genome form five main families. Phylogenetic analysis, paralogon groups, and fingerprints. *Molecular Pharmacology*, *63*(6), 1256–1272.

Freund, T. F., Katona, I., & Piomelli, D. (2003). Role of endogenous cannabinoids in synaptic signaling. *Physiological Reviews*, *83*(3), 1017–1066.

Fritze, O., Filipek, S., Kuksa, V., Palczewski, K., Hofmann, K. P., & Ernst, O. P. (2003). Role of the conserved NPxxY(x)5,6F motif in the rhodopsin ground state and during activation. *Proceedings of the National Academy of Sciences of the United States of America*, *100*(5), 2290–2295.

Fukami, M., Suzuki, E., Igarashi, M., Miyado, M., & Ogata, T. (2018). Gain-of-function mutations in G-protein-coupled receptor genes associated with human endocrine disorders. *Clinical Endocrinology*, *88*(3), 351–359.

George, D. C. P., Chakraborty, C., Haneef, S. S., NagaSundaram, N., Chen, L., & Zhu, H. (2014). Evolution- and Structure-Based Computational Strategy Reveals the Impact

of Deleterious Missense Mutations on MODY 2 (Maturity-Onset Diabetes of the Young, Type 2). *Theranostics*, *4*(4), 366–385.

Gohlke, H. & Case, D. (2004). Converging Free Energy Estimates: MM-PB(GB)SA Studies on the Protein−protein Complex Ras−Raf. *Journal of Computational Chemistry, 25*(2), 238−250.

Gong, J.-P., Onaivi, E. S., Ishiguro, H., Liu, Q.-R., Tagliaferro, P. A., Brusco, A., & Uhl, G. R. (2006). Cannabinoid CB2 receptors: immunohistochemical localization in rat brain. *Brain Research*, *1071*(1), 10–23.

Grossfield, A., Pitman, M. C., Feller, S. E., Soubias, O., & Gawrisch, K. (2008). Internal hydration increases during activation of the G-protein-coupled receptor rhodopsin. *Journal of Molecular Biology*, *381*(2), 478–486.

Gyombolai, P., Tóth, A. D., Tímár, D., Turu, G., & Hunyady, L. (2015). Mutations in the "DRY" motif of the CB1 cannabinoid receptor result in biased receptor variants. *Journal of Molecular Endocrinology*, *54*(1), 75–89.

Habib, A. M., Okorokov, A. L., Hill, M. N., Bras, J. T., Lee, M.-C., Li, S., … Cox, J. J. (2019). Microdeletion in a FAAH pseudogene identified in a patient with high anandamide concentrations and pain insensitivity. *British Journal of Anaesthesia*, (In press).

Hanlon, C. D., & Andrew, D. J. (2015). Outside-in signaling--a brief review of GPCR signaling with a focus on the Drosophila GPCR family. *Journal of Cell Science*, *128*(19), 3533–3542.

Hardianto, A., Khanna, V., Liu, F., & Ranganathan, S. (2019). Diverse dynamics features of novel protein kinase C (PKC) isozymes determine the selectivity of a fluorinated balanol analogue for PKCε. *BMC Bioinformatics*, *19*(Suppl 13), 342.

Hauser, A. S., Chavali, S., Masuho, I., Jahn, L. J., Martemyanov, K. A., Gloriam, D. E., & Babu, M. M. (2018). Pharmacogenomics of GPCR Drug Targets. *Cell*, *172*(1–2), 41-54.e19.

Herkenham, M., Lynn, A. B., Johnson, M. R., Melvin, L. S., de Costa, B. R., & Rice, K. C. (1991). Characterization and localization of cannabinoid receptors in rat brain: a quantitative in vitro autoradiographic study. *The Journal of Neuroscience: The Official Journal of the Society for Neuroscience*, *11*(2), 563–583.

Hillard, C. J., Muthian, S., & Kearn, C. S. (1999). Effects of CB1 cannabinoid receptor activation on cerebellar granule cell nitric oxide synthase activity. *FEBS Letters*, *459*(2), 277–281.

Hoehe, M. R., Caenazzo, L., Martinez, M. M., Hsieh, W. T., Modi, W. S., Gershon, E. S., & Bonner, T. I. (1991). Genetic and physical mapping of the human cannabinoid receptor gene to chromosome 6q14-q15. *The New Biologist*, *3*(9), 880–885.

Hopfer, C. J., Young, S. E., Purcell, S., Crowley, T. J., Stallings, M. C., Corley, R. P., … Ehringer, M. A. (2006). Cannabis receptor haplotype associated with fewer cannabis dependence symptoms in adolescents. *American Journal of Medical Genetics. Part B, Neuropsychiatric Genetics: The Official Publication of the International Society of Psychiatric Genetics*, *141B*(8), 895–901.

Hourani, W., & Alexander, S. P. H. (2018). Cannabinoid ligands, receptors and enzymes: Pharmacological tools and therapeutic potential. *Brain and Neuroscience Advances*, *2*, 2398212818783908.

Howlett, A. C. (1995). Pharmacology of cannabinoid receptors. *Annual Review of Pharmacology and Toxicology*, *35*, 607–634.

Howlett, A. C., Barth, F., Bonner, T. I., Cabral, G., Casellas, P., Devane, W. A., … Pertwee, R. G. (2002). International Union of Pharmacology. XXVII. Classification of cannabinoid receptors. *Pharmacological Reviews*, *54*(2), 161–202.

Howlett, A. C., Johnson, M. R., & Melvin, L. S. (1990). Classical and nonclassical cannabinoids: mechanism of action--brain binding. *NIDA Research Monograph*, *96*, 100–111.

Hua, T., Vemuri, K., Nikas, S. P., Laprairie, R. B., Wu, Y., Qu, L., … Liu, Z.-J. (2017). Crystal structures of agonist-bound human cannabinoid receptor CB1. *Nature*, *547*(7664), 468–471.

Hua, T., Vemuri, K., Pu, M., Qu, L., Han, G. W., Wu, Y., … Liu, Z.-J. (2016). Crystal Structure of the Human Cannabinoid Receptor CB1. *Cell*, *167*(3), 750-762.e14.

Huang, W., Manglik, A., Venkatakrishnan, A. J., Laeremans, T., Feinberg, E. N., Sanborn, A. L., … Kobilka, B. K. (2015). Structural insights into μ-opioid receptor activation. *Nature*, *524*(7565), 315–321.

Huynh, T., Khan, J. M., & Ranganathan, S. (2011). A comparative structural bioinformatics analysis of inherited mutations in β-D-Mannosidase across multiple species reveals a genotype-phenotype correlation. *BMC Genomics*, *12 Suppl 3*, S22.

Ibsen, M. S., Connor, M., & Glass, M. (2017). Cannabinoid CB1 and CB2 Receptor Signaling and Bias. *Cannabis and Cannabinoid Research*, *2*(1), 48–60.

Icick, R., Peoc'h, K., Karsinti, E., Ksouda, K., Hajj, A., Bloch, V., … Vorspan, F. (2015). A cannabinoid receptor 1 polymorphism is protective against major depressive disorder in methadone-maintained outpatients. *The American Journal on Addictions*, *24*(7), 613–620.

Isir, A. B., Baransel, C., & Nacak, M. (2016). An Information Theoretical Study of the Epistasis Between the CNR1 1359 G/A Polymorphism and the Taq1A and Taq1B DRD2 Polymorphisms: Assessing the Susceptibility to Cannabis Addiction in a Turkish Population. *Journal of Molecular Neuroscience: MN*, *58*(4), 456–460.

Iversen, L. (2003). Cannabis and the brain. *Brain*, *126*(6), 1252–1270.

Iversen, L. (2009). The Science of Marijuana, 2nd edn. *British Journal of Clinical Pharmacology*, *67*(2), 268.

Jiang, Y., Nie, Y., Li, Y., & Zhang, L. (2014). Association of cannabinoid type 1 receptor and fatty acid amide hydrolase genetic polymorphisms in Chinese patients with irritable bowel syndrome. *Journal of Gastroenterology and Hepatology*, *29*(6), 1186–1191.

Jo, S., Kim, T., & Im, W. (2007). Automated Builder and Database of Protein/Membrane Complexes for Molecular Dynamics Simulations. *PLOS ONE*, *2*(9), e880.

Jo, S., Kim, T., Iyer, V. G., & Im, W. (2008). CHARMM-GUI: A web-based graphical user interface for CHARMM. *Journal of Computational Chemistry*, *29*(11), 1859–1865.

Johnson, M. R., & Melvin, L. S. (1986). The discovery of nonclassical cannabinoid analgetics. *In: Mechoulam. R (ed.): Cannabinoids as Therapeutic Agents* (CRC Press, Boca Raton, FL), 121–145.

Jorgensen, W. L., Chandrasekhar, J., Madura, J. D., Impey, R. W., & Klein, M. L. (1983). Comparison of simple potential functions for simulating liquid water. *The Journal of Chemical Physics*, *79*(2), 926–935.

Julian, B., Gao, K., Harwood, B. N., Beinborn, M., & Kopin, A. S. (2017). Mutation-Induced Functional Alterations of CCR6. *The Journal of Pharmacology and Experimental Therapeutics*, *360*(1), 106–116.

Jung, S. W., Cho, A. E., & Yu, W. (2018). Exploring the Ligand Efficacy of Cannabinoid Receptor 1 (CB1) using Molecular Dynamics Simulations. *Scientific Reports*, *8*(1), 13787.

Kano, M., Ohno-Shosaku, T., Hashimotodani, Y., Uchigashima, M., & Watanabe, M. (2009). Endocannabinoid-mediated control of synaptic transmission. *Physiological Reviews*, *89*(1), 309–380.

Katona, I., & Freund, T. F. (2012). Multiple functions of endocannabinoid signaling in the brain. *Annual Review of Neuroscience*, *35*, 529–558.

Katritch, V., Cherezov, V., & Stevens, R. C. (2013). Structure-Function of the G-protein-Coupled Receptor Superfamily. *Annual Review of Pharmacology and Toxicology*, *53*, 531–556.

Kazius, J., Wurdinger, K., van Iterson, M., Kok, J., Bäck, T., & Ijzerman, A. P. (2008). GPCR NaVa database: natural variants in human G protein-coupled receptors. *Human Mutation*, *29*(1), 39–44.

Khan, J. M., & Ranganathan, S. (2009). A multi-species comparative structural bioinformatics analysis of inherited mutations in α-D-Mannosidase reveals strong genotype-phenotype correlation. *BMC Genomics*, *10*(Suppl 3), S33.

Kitchen, D. B., Decornez, H., Furr, J. R., & Bajorath, J. (2004). Docking and scoring in virtual screening for drug discovery: methods and applications. *Nature Reviews. Drug Discovery*, *3*(11), 935–949.

Knapman, A., & Connor, M. (2015). Cellular signalling of non-synonymous single-nucleotide polymorphisms of the human μ-opioid receptor (OPRM1). *British Journal of Pharmacology*, *172*(2), 349–363.

Knapman, A., Santiago, M., & Connor, M. (2015). A6V polymorphism of the human μ-opioid receptor decreases signalling of morphine and endogenous opioids in vitro. *British Journal of Pharmacology*, *172*(9), 2258–2272.

Kohlhoff, K. J., Shukla, D., Lawrenz, M., Bowman, G. R., Konerding, D. E., Belov, D., … Pande, V. S. (2014). Cloud-based simulations on Google Exacycle reveal ligand modulation of GPCR activation pathways. *Nature Chemistry*, *6*(1), 15–21.

Krishna Kumar, K., Shalev-Benami, M., Robertson, M. J., Hu, H., Banister, S. D., Hollingsworth, S. A., … Skiniotis, G. (2019). Structure of a Signaling Cannabinoid Receptor 1-G Protein Complex. *Cell*, *176*(3), 448-458.e12.

Kumari, P., Ghosh, E., & Shukla, A. K. (2015). Emerging Approaches to GPCR Ligand Screening for Drug Discovery. *Trends in Molecular Medicine*, *21*(11), 687–701.

Laprairie, R. B., Kelly, M. E. M., & Denovan-Wright, E. M. (2012). The dynamic nature of type 1 cannabinoid receptor (CB(1)) gene transcription. *British Journal of Pharmacology*, *167*(8), 1583–1595.

Lauckner, J. E., Jensen, J. B., Chen, H.-Y., Lu, H.-C., Hille, B., & Mackie, K. (2008). GPR55 is a cannabinoid receptor that increases intracellular calcium and inhibits M current. *Proceedings of the National Academy of Sciences of the United States of America*, *105*(7), 2699–2704.

Lester, K. J., Coleman, J. R. I., Roberts, S., Keers, R., Breen, G., Bögels, S., … Eley, T. C. (2017). Genetic variation in the endocannabinoid system and response to Cognitive Behavior Therapy for child anxiety disorders. *American Journal of Medical Genetics. Part B, Neuropsychiatric Genetics: The Official Publication of the International Society of Psychiatric Genetics*, *174*(2), 144–155.

Lin, H., Sassano, M. F., Roth, B. L., & Shoichet, B. K. (2013). A pharmacological organization of G protein–coupled receptors. *Nature Methods*, *10*(2), 140–146.

Lomize, M. A., Pogozheva, I. D., Joo, H., Mosberg, H. I., & Lomize, A. L. (2012). OPM database and PPM web server: resources for positioning of proteins in membranes. *Nucleic Acids Research*, *40*(Database issue), D370-376.

López-Moreno, J. A., Echeverry-Alzate, V., & Bühler, K.-M. (2012). The genetic basis of the endocannabinoid system and drug addiction in humans. *Journal of Psychopharmacology (Oxford, England)*, *26*(1), 133–143.

Lu, H.-C., & Mackie, K. (2016). An Introduction to the Endogenous Cannabinoid System. *Biological Psychiatry*, *79*(7), 516–525.

Maccarrone, M., Bab, I., Bíró, T., Cabral, G. A., Dey, S. K., Di Marzo, V., … Zimmer, A. (2015). Endocannabinoid signaling at the periphery: 50 years after THC. *Trends in Pharmacological Sciences*, *36*(5), 277–296.

Maier, J. A., Martinez, C., Kasavajhala, K., Wickstrom, L., Hauser, K. E., & Simmerling, C. (2015). ff14SB: Improving the Accuracy of Protein Side Chain and Backbone Parameters from ff99SB. *Journal of Chemical Theory and Computation*, *11*(8), 3696–3713.

Mallipeddi, S., Janero, D. R., Zvonok, N., & Makriyannis, A. (2017). Functional selectivity at G-protein coupled receptors: Advancing cannabinoid receptors as drug targets. *Biochemical Pharmacology*, *128*, 1–11.

Mallory, D. P., Gutierrez, E., Pinkevitch, M., Klinginsmith, C., Comar, W. D., Roushar, F. J., … Jastrzebska, B. (2018). The Retinitis Pigmentosa-Linked Mutations in Transmembrane Helix 5 of Rhodopsin Disrupt Cellular Trafficking Regardless of Oligomerization State. *Biochemistry*, *57*(35), 5188–5201.

Matsuda, L. A., Lolait, S. J., Brownstein, M. J., Young, A. C., & Bonner, T. I. (1990). Structure of a cannabinoid receptor and functional expression of the cloned cDNA. *Nature*, *346*(6284), 561–564.

Matsunaga, M., Isowa, T., Yamakawa, K., Fukuyama, S., Shinoda, J., Yamada, J., & Ohira, H. (2014). Genetic Variations in the Human Cannabinoid Receptor Gene Are Associated with Happiness. *PLoS ONE*, *9*(4).

McAllister, S. D., Tao, Q., Barnett-Norris, J., Buehner, K., Hurst, D. P., Guarnieri, F., … Abood, M. E. (2002). A critical role for a tyrosine residue in the cannabinoid receptors for ligand recognition. *Biochemical Pharmacology*, *63*(12), 2121–2136.

Mecha, M., Feliú, A., Carrillo-Salinas, F. J., Rueda-Zubiaurre, A., Ortega-Gutiérrez, S., de Sola, R. G., & Guaza, C. (2015). Endocannabinoids drive the acquisition of an alternative phenotype in microglia. *Brain, Behavior, and Immunity*, *49*, 233–245.

Mechoulam, R., Ben-Shabat, S., Hanus, L., Ligumsky, M., Kaminski, N. E., Schatz, A. R., … Vogel, Z. (1995). Identification of an endogenous 2-monoglyceride, present in canine gut, that binds to cannabinoid receptors. *Biochemical Pharmacology*, *50*(1), 83–90.

Melroy-Greif, W. E., Wilhelmsen, K. C., & Ehlers, C. L. (2016). Genetic variation in FAAH is associated with cannabis use disorders in a young adult sample of Mexican Americans. *Drug and Alcohol Dependence*, *166*, 249–253.

Miller, L. K., & Devi, L. A. (2011). The highs and lows of cannabinoid receptor expression in disease: mechanisms and their therapeutic implications. *Pharmacological Reviews*, *63*(3), 461–470.

Min, L., Nie, M., Zhang, A., Wen, J., Noel, S. D., Lee, V., … Kaiser, U. B. (2016). Computational analysis of missense variants of G protein-coupled receptors involved in the neuroendocrine regulation of reproduction. *Neuroendocrinology*, *103*(3–4), 230–239.

MODELLER A Program for Protein Structure Modeling Release 9.21, r11301. https://salilab.org/modeller/manual/

Monteleone, P., Bifulco, M., Di Filippo, C., Gazzerro, P., Canestrelli, B., Monteleone, F., … Maj, M. (2009). Association of CNR1 and FAAH endocannabinoid gene polymorphisms with anorexia nervosa and bulimia nervosa: evidence for synergistic effects. *Genes, Brain, and Behavior*, *8*(7), 728–732.

Monteleone, Palmiero, Milano, W., Petrella, C., Canestrelli, B., & Maj, M. (2010). Endocannabinoid Pro129Thr FAAH functional polymorphism but not 1359G/A CNR1 polymorphism is associated with antipsychotic-induced weight gain. *Journal of Clinical Psychopharmacology*, *30*(4), 441–445.

Moreira, I. S. (2014). Structural features of the G-protein/GPCR interactions. *Biochimica Et Biophysica Acta*, *1840*(1), 16–33.

Müller, G. (2000). Towards 3D structures of G protein-coupled receptors: a multidisciplinary approach. *Current Medicinal Chemistry*, *7*(9), 861-888.

Munk C, Mutt E, Isberg V, Nikolajsen LF, Bibbe JM, Flock T, Hanson MA, Stevens RC, Deupi X., & Gloriam DE. (2019). An online resource for GPCR structure determination and analysis. *Nature Methods, 16*(2), 151-162.

Munro, S., Thomas, K. L., & Abu-Shaar, M. (1993). Molecular characterization of a peripheral receptor for cannabinoids. *Nature*, *365*(6441), 61-65.

Neves, M. A. C., Totrov, M., & Abagyan, R. (2012). Docking and scoring with ICM: the benchmarking results and strategies for improvement. *Journal of Computer-Aided Molecular Design*, *26*(6), 675–686.

Newport, T. D., Sansom, M. S. P., & Stansfeld, P. J. (2019). The MemProtMD database: a resource for membrane-embedded protein structures and their lipid interactions. *Nucleic Acids Research*, *47*(D1), D390–D397.

Niroula, A., Urolagin, S., & Vihinen, M. (2015). PON-P2: prediction method for fast and reliable identification of harmful variants. *PloS One*, *10*(2), e0117380.

Nygaard, R., Frimurer, T. M., Holst, B., Rosenkilde, M. M., & Schwartz, T. W. (2009). Ligand binding and micro-switches in 7TM receptor structures. *Trends in Pharmacological Sciences*, *30*(5), 249–259.

O'Sullivan, S. E. (2007). Cannabinoids go nuclear: evidence for activation of peroxisome proliferator-activated receptors. *British Journal of Pharmacology*, *152*(5), 576–582.

Oddi, S., Dainese, E., Sandiford, S., Fezza, F., Lanuti, M., Chiurchiù, V., … Maccarrone, M. (2012). Effects of palmitoylation of Cys(415) in helix 8 of the CB(1) cannabinoid receptor on membrane localization and signalling. *British Journal of Pharmacology*, *165*(8), 2635–2651.

Ohno-Shosaku, T., Maejima, T., & Kano, M. (2001). Endogenous Cannabinoids Mediate Retrograde Signals from Depolarized Postsynaptic Neurons to Presynaptic Terminals. *Neuron*, *29*(3), 729–738.

Pacher, P., Bátkai, S., & Kunos, G. (2006). The endocannabinoid system as an emerging target of pharmacotherapy. *Pharmacological Reviews*, *58*(3), 389–462.

Pagotto, U., & Pasquali, R. (2005). Fighting obesity and associated risk factors by antagonising cannabinoid type 1 receptors. *Lancet (London, England)*, *365*(9468), 1363–1364.

Pagotto, U., Vicennati, V., & Pasquali, R. (2005). The endocannabinoid system and the treatment of obesity. *Annals of Medicine*, *37*(4), 270–275.

Palczewski, K., Kumasaka, T., Hori, T., Behnke, C. A., Motoshima, H., Fox, B. A., … Miyano, M. (2000). Crystal structure of rhodopsin: A G protein-coupled receptor. *Science (New York, N.Y.)*, *289*(5480), 739–745.

Pándy-Szekeres, G., Munk, C., Tsonkov, T. M., Mordalski, S., Harpsøe, K., Hauser, A. S., … Gloriam, D. E. (2018). GPCRdb in 2018: adding GPCR structure models and ligands. *Nucleic Acids Research*, *46*(D1), D440–D446.

Pertwee, R. G., Howlett, A. C., Abood, M. E., Alexander, S. P. H., Di Marzo, V., Elphick, M. R., … Ross, R. A. (2010). International Union of Basic and Clinical Pharmacology. LXXIX. Cannabinoid receptors and their ligands: beyond CB□ and CB□. *Pharmacological Reviews*, *62*(4), 588–631.

Pertwee, Roger G. (2002). Cannabinoids and multiple sclerosis. *Pharmacology & Therapeutics*, *95*(2), 165–174.

Pisanu, C., Congiu, D., Costa, M., Sestu, M., Chillotti, C., Ardau, R., … Del Zompo, M. (2013). No association of endocannabinoid genes with bipolar disorder or lithium response in a Sardinian sample. *Psychiatry Research*, *210*(3), 887–890.

Pistis, M., & Melis, M. (2010). From surface to nuclear receptors: the endocannabinoid family extends its assets. *Current Medicinal Chemistry*, *17*(14), 1450–1467.

Pryce, G., & Baker, D. (2015). Endocannabinoids in Multiple Sclerosis and Amyotrophic Lateral Sclerosis. *Handbook of Experimental Pharmacology*, *231*, 213–231.

Radwan, M., Ross, S., Slade, D., Ahmed, S., Zulfiqar, F., & ElSohly, M. (2008). Isolation and Characterization of New Cannabis Constituents from a High Potency Variety. *Planta Medica*, *74*(3), 267–272.

Reggio, P. H. (2010). Endocannabinoid binding to the cannabinoid receptors: what is known and what remains unknown. *Current Medicinal Chemistry*, *17*(14), 1468–1486.

Rinaldi-Carmona, M., Barth, F., Héaulme, M., Shire, D., Calandra, B., Congy, C., … Caput, D. (1994). SR141716A, a potent and selective antagonist of the brain cannabinoid receptor. *FEBS Letters*, *350*(2–3), 240–244.

Rinaldi-Carmona, M., Le Duigou, A., Oustric, D., Barth, F., Bouaboula, M., Carayon, P., … Le Fur, G. (1998). Modulation of CB1 cannabinoid receptor functions after a long-term exposure to agonist or inverse agonist in the Chinese hamster ovary cell expression system. *The Journal of Pharmacology and Experimental Therapeutics*, *287*(3), 1038–1047.

Roche, J. P., Bounds, S., Brown, S., & Mackie, K. (1999). A mutation in the second transmembrane region of the CB1 receptor selectively disrupts G protein signaling and prevents receptor internalization. *Molecular Pharmacology*, *56*(3), 611–618.

Rodrigues, C. H., Pires, D. E., & Ascher, D. B. (2018). DynaMut: predicting the impact of mutations on protein conformation, flexibility and stability. *Nucleic Acids Research*, *46*(W1), W350–W355.

Roe, D. R., & Cheatham, T. E. (2013). PTRAJ and CPPTRAJ: Software for Processing and Analysis of Molecular Dynamics Trajectory Data. *Journal of Chemical Theory and Computation*, *9*(7), 3084–3095.

Russo, P., Strazzullo, P., Cappuccio, F. P., Tregouet, D. A., Lauria, F., Loguercio, M., … Siani, A. (2007). Genetic variations at the endocannabinoid type 1 receptor gene (CNR1) are associated with obesity phenotypes in men. *The Journal of Clinical Endocrinology and Metabolism*, *92*(6), 2382–2386.

Ryberg, E., Larsson, N., Sjögren, S., Hjorth, S., Hermansson, N.-O., Leonova, J., … Greasley, P. J. (2007). The orphan receptor GPR55 is a novel cannabinoid receptor. *British Journal of Pharmacology*, *152*(7), 1092–1101.

Ryckaert, J.-P., Ciccotti, G., & Berendsen, H. J. C. (1977). Numerical integration of the cartesian equations of motion of a system with constraints: molecular dynamics of n-alkanes. *Journal of Computational Physics*, *23*(3), 327–341.

Sabatucci, A., Tortolani, D., Dainese, E., & Maccarrone, M. (2018). In silico mapping of allosteric ligand binding sites in type-1 cannabinoid receptor. *Biotechnolology and Applied Biochemistry, 65*(1):21-28.

Salzet, M., Breton, C., Bisogno, T., & Di Marzo, V. (2000). Comparative biology of the endocannabinoid system possible role in the immune response. *European Journal of Biochemistry*, *267*(16), 4917–4927.

Scheen, A. J. (2007). Cannabinoid-1 receptor antagonists in type-2 diabetes. *Best Practice & Research. Clinical Endocrinology & Metabolism*, *21*(4), 535–553.

Schöneberg, T., Schulz, A., Biebermann, H., Hermsdorf, T., Römpler, H., & Sangkuhl, K. (2004). Mutant G-protein-coupled receptors as a cause of human diseases. *Pharmacology & Therapeutics*, *104*(3), 173–206.

Sengupta, D., Sonar, K., & Joshi, M. (2017). Characterizing clinically relevant natural variants of GPCRs using computational approaches. *Methods in Cell Biology*, *142*, 187–204.

Sensoy, O., Almeida, J. G., Shabbir, J., Moreira, I. S., & Morra, G. (2017). Computational studies of G protein-coupled receptor complexes: Structure and dynamics. *Methods in Cell Biology*, *142*, 205–245.

Shao, Z., Yin, J., Chapman, K., Grzemska, M., Clark, L., Wang, J., & Rosenbaum, D. M. (2016). High-resolution crystal structure of the human CB1 cannabinoid receptor. *Nature*, *540*(7634), 602–606.

Sherry, S. T., Ward, M. H., Kholodov, M., Baker, J., Phan, L., Smigielski, E. M., & Sirotkin, K. (2001). dbSNP: the NCBI database of genetic variation. *Nucleic Acids Research*, *29*(1), 308–311.

Shim, J.-Y. (2010). Understanding Functional Residues of the Cannabinoid CB1 Receptor for Drug Discovery. *Current Topics in Medicinal Chemistry*, *10*(8), 779–798.

Shim, J.-Y., & Padgett, L. (2013). Functional residues essential for the activation of the CB1 cannabinoid receptor. *Methods in Enzymology*, *520*, 337–355.

Shim, J.-Y., Ahn, K. H., & Kendall, D. A. (2013). Molecular Basis of Cannabinoid CB1 Receptor Coupling to the G Protein Heterotrimer Gαiβγ IDENTIFICATION OF KEY CB1 CONTACTS WITH THE C-TERMINAL HELIX α5 OF Gαi. *Journal of Biological Chemistry*, *288*(45), 32449–32465.

Shim, J.-Y., Bertalovitz, A. C., & Kendall, D. A. (2011). Identification of essential cannabinoid-binding domains: structural insights into early dynamic events in receptor activation. *The Journal of Biological Chemistry*, *286*(38), 33422–33435.

Showalter, V. M., Compton, D. R., Martin, B. R., & Abood, M. E. (1996). Evaluation of binding in a transfected cell line expressing a peripheral cannabinoid receptor (CB2): identification of cannabinoid receptor subtype selective ligands. *The Journal of Pharmacology and Experimental Therapeutics*, *278*(3), 989–999.

Smith, D. R., Stanley, C. M., Foss, T., Boles, R. G., & McKernan, K. (2017). Rare genetic variants in the endocannabinoid system genes CNR1 and DAGLA are associated with neurological phenotypes in humans. *PloS One*, *12*(11), e0187926.

Smith, S. O. (2012). Insights into the activation mechanism of the visual receptor rhodopsin. *Biochemical Society Transactions*, *40*(2), 389–393.

Stella, N. (2009). Endocannabinoid signaling in microglial cells. *Neuropharmacology*, *56 Suppl 1*, 244–253.

Studer, R. A., Dessailly, B. H., & Orengo, C. A. (2013). Residue mutations and their impact on protein structure and function: detecting beneficial and pathogenic changes. *The Biochemical Journal*, *449*(3), 581–594.

Sugiura, T., Kondo, S., Sukagawa, A., Nakane, S., Shinoda, A., Itoh, K., … Waku, K. (1995). 2-Arachidonoylgylcerol: A possible endogenous cannabinoid receptor ligand in brain. *Biochemical and Biophysical Research Communications*, *215*(1), 89–97.

Svízenská, I., Dubový, P., & Sulcová, A. (2008). Cannabinoid receptors 1 and 2 (CB1 and CB2), their distribution, ligands and functional involvement in nervous system structures--a short review. *Pharmacology, Biochemistry, and Behavior*, *90*(4), 501–511.

Tandale, A., Joshi, M., & Sengupta, D. (2016). Structural insights and functional implications of inter-individual variability in β_2-adrenergic receptor. *Scientific Reports*, *6*, 24379.

Thusberg J, Olatubosun A, Vihinen M. (2011). Performance of mutation pathogenicity prediction methods on missense variants. *Human Mutation, 32*(4), 358–368.

Tiwari, A. K., Zai, C. C., Likhodi, O., Lisker, A., Singh, D., Souza, R. P., … Müller, D. J. (2010). A Common Polymorphism in the Cannabinoid Receptor 1 (CNR1) Gene is Associated with Antipsychotic-Induced Weight Gain in Schizophrenia. *Neuropsychopharmacology*, *35*(6), 1315–1324.

Totrov, M., & Abagyan, R. (1997). Flexible protein-ligand docking by global energy optimization in internal coordinates. *Proteins*, *Suppl 1*, 215–220.

Turner, C. E., Bouwsma, O. J., Billets, S., & Elsohly, M. A. (1980). Constituents of Cannabis sativa L. XVIII--Electron voltage selected ion monitoring study of cannabinoids. *Biomedical Mass Spectrometry*, *7*(6), 247–256.

Turner, P. J. (2005). XMGRACE, Version 5.1. 19. Center for Coastal and Land-Margin Research, *Oregon Graduate Institute of Science and Technology,* Beaverton OR.

Ujike, H., Takaki, M., Nakata, K., Tanaka, Y., Takeda, T., Kodama, M., … Kuroda, S. (2002). CNR1, central cannabinoid receptor gene, associated with susceptibility to hebephrenic schizophrenia. *Molecular Psychiatry*, *7*(5), 515–518.

Ulfers, A. L., McMurry, J. L., Miller, A., Wang, L., Kendall, D. A., & Mierke, D. F. (2002). Cannabinoid receptor-G protein interactions: Gαi1-bound structures of IC3 and a mutant with altered G protein specificity. *Protein Science : A Publication of the Protein Society*, *11*(10), 2526–2531.

Vanommeslaeghe, K., & MacKerell, A. D. (2012). Automation of the CHARMM General Force Field (CGenFF) I: bond perception and atom typing. *Journal of Chemical Information and Modeling*, *52*(12), 3144–3154.

Vanommeslaeghe, K., Hatcher, E., Acharya, C., Kundu, S., Zhong, S., Shim, J., … Mackerell, A. D. (2010). CHARMM general force field: A force field for drug-like molecules compatible with the CHARMM all-atom additive biological force fields. *Journal of Computational Chemistry*, *31*(4), 671–690.

Vanommeslaeghe, K., Raman, E. P., & MacKerell, A. D. (2012). Automation of the CHARMM General Force Field (CGenFF) II: assignment of bonded parameters and partial atomic charges. *Journal of Chemical Information and Modeling*, *52*(12), 3155–3168.

Venkatakrishnan, A. J., Deupi, X., Lebon, G., Tate, C. G., Schertler, G. F., & Babu, M. M. (2013). Molecular signatures of G-protein-coupled receptors. *Nature*, *494*(7436), 185–194.

Villanueva, M. T. (2018). Pharmacogenomics: Know your GPCR mutations (and target them right). *Nature Reviews Drug Discovery*, *17*, 94.

Vogel, R., Mahalingam, M., Lüdeke, S., Huber, T., Siebert, F., & Sakmar, T. P. (2008). Functional role of the "ionic lock"--an interhelical hydrogen-bond network in family A heptahelical receptors. *Journal of Molecular Biology*, *380*(4), 648–655.

Wang, J., Wolf, R. M., Caldwell, J. W., Kollman, P. A., & Case, D. A. (2004). Development and testing of a general amber force field. *Journal of Computational Chemistry*, *25*(9), 1157–1174.

Warszycki D, Rueda M, Mordalski S, Kristiansen K, Satala G, Rataj K, Chilmonczyk Z, Sylte I, Abagyan R, Bojarski AJ. (2017). From Homology Models to a Set of Predictive Binding Pockets–a 5-HT1A Receptor Case Study. *Journal of Chemical Information and Modeling, 57*(2), 311-321

Webb, B., & Sali, A. (2016). Comparative Protein Structure Modeling Using MODELLER. *Current Protocols in Bioinformatics*, *54*, 5.6.1-5.6.37.

Weiser, J., Shenkin, P. S., & Still, W. C. (1999). Approximate atomic surfaces from linear combinations of pairwise overlaps (LCPO). *Journal of Computational Chemistry*, *20*(2), 217–230.

Wickert, M., Hildick, K. L., Baillie, G. L., Jelinek, R., Aparisi Rey, A., Monory, K., … Lutz, B. (2018). The F238L Point Mutation in the Cannabinoid Type 1 Receptor Enhances Basal Endocytosis via Lipid Rafts. *Frontiers in Molecular Neuroscience*, *11*, 230.

Wierzbicki, A. S. (2006). Rimonabant: endocannabinoid inhibition for the metabolic syndrome. *International Journal of Clinical Practice*, *60*(12), 1697–1706.

Wilson, R. I., & Nicoll, R. A. (2001). Endogenous cannabinoids mediate retrograde signalling at hippocampal synapses. *Nature*, *410*(6828), 588–592.

Worth, C. L., Kreuchwig, A., Kleinau, G., & Krause, G. (2011). GPCR-SSFE: a comprehensive database of G-protein-coupled receptor template predictions and homology models. *BMC Bioinformatics*, *12*, 185.

Wu, E. L., Cheng, X., Jo, S., Rui, H., Song, K. C., Dávila□Contreras, E. M., … Im, W. (2014). CHARMM-GUI Membrane Builder toward realistic biological membrane simulations. *Journal of Computational Chemistry*, *35*(27), 1997–2004.

Xiang, J., Chun, E., Liu, C., Jing, L., Al-Sahouri, Z., Zhu, L., & Liu, W. (2016). Successful Strategies to Determine High-Resolution Structures of GPCRs. *Trends in Pharmacological Sciences*, *37*(12), 1055–1069.

Xie, X. Q., Melvin, L. S., & Makriyannis, A. (1996). The conformational properties of the highly selective cannabinoid receptor ligand CP-55,940. *The Journal of Biological Chemistry*, *271*(18), 10640–10647.

Yao, Y., Xu, Y., Zhao, J., Ma, Y., Su, K., Yuan, W., … Li, M. D. (2018). Detection of Significant Association Between Variants in Cannabinoid Receptor 1 Gene (CNR1) and Personality in African-American Population. *Frontiers in Genetics*, *9*, 199.

Zhang, P.-W., Ishiguro, H., Ohtsuki, T., Hess, J., Carillo, F., Walther, D., … Uhl, G. R. (2004). Human cannabinoid receptor 1: 5' exons, candidate regulatory regions, polymorphisms, haplotypes and association with polysubstance abuse. *Molecular Psychiatry*, *9*(10), 916–931.

Zou, S., & Kumar, U. (2018). Cannabinoid Receptors and the Endocannabinoid System: Signaling and Function in the Central Nervous System. *International Journal of Molecular Sciences*, *19*(3), 833.

Zuo, L., Kranzler, H. R., Luo, X., Covault, J., & Gelernter, J. (2007). CNR1 variation modulates risk for drug and alcohol dependence. *Biological Psychiatry*, *62*(6), 616–626.

Supplementary material

Supplementary Table 1. **List of predicted SNPs**. Variants are sorted based on prediction score and the availability of structural information.

S.No	SNP ID	Variant	PredictSNP (Confidence)	PON-P2 (Probability)	Meta-SNP (Confidence)	Structure available (Y/N)
1	GPCRdb	D163E	Deleterious (76%)	Pathogenic (0.91)	Disease (0.94)	Y
2	GPCRdb	D163N	Deleterious (76%)	Pathogenic (0.91)	Disease (0.92)	Y
3	rs748199661	D163Y	Deleterious (87%)	Pathogenic (0.92)	Disease (0.94)	Y
4	GPCRdb	K192E	Deleterious (87%)	Pathogenic (0.88)	Disease (0.76)	Y
5	GPCRdb	C257A	Deleterious (87%)	Pathogenic (0.84)	Disease (0.84)	Y
6	GPCRdb	C264A	Deleterious (76%)	Pathogenic (0.82)	Disease (0.88)	Y
7	GPCRdb	Y275F	Deleterious (87%)	Pathogenic (0.77)	Disease (0.68)	Y
8	rs757316503	W299R	Deleterious (87%)	Pathogenic (0.92)	Disease (0.78)	Y
9	rs763132752	R336C	Deleterious (87%)	Pathogenic (0.93)	Disease (0.81)	Y
10	GPCRdb	C355A	Deleterious (76%)	Pathogenic (0.84)	Disease (0.83)	Y
11	GPCRdb	M363A	Deleterious (76%)	Pathogenic (0.96)	Disease (0.52)	Y
12	rs907130013	Y397C	Deleterious (87%)	Pathogenic (0.95)	Disease (0.87)	Y
13	GPCRdb	C107A	Deleterious (64%)	Pathogenic (0.84)	Disease (0.71)	Y
14	rs756727581	P151A	Deleterious (51%)	Pathogenic (0.85)	Disease (0.65)	Y
15	rs368199704	G157C	Deleterious (72%)	Pathogenic (0.84)	Disease (0.53)	Y
16	rs759310920	A160V	Deleterious (61%)	Pathogenic (0.84)	Disease (0.77)	Y
17	GPCRdb	F174A	Deleterious (72%)	Pathogenic (0.89)	Disease (0.67)	Y
18	rs779597655	V179M	Deleterious (51%)	Pathogenic (0.98)	Neutral (0.48)	Y
19	rs757730631	S185N	Deleterious (51%)	Pathogenic (0.88)	Neutral (0.44)	Y
20	GPCRdb	F189A	Deleterious (61%)	Pathogenic (0.89)	Disease (0.72)	Y
21	GPCRdb	K192A	Deleterious (51%)	Pathogenic (0.85)	Neutral (0.49)	Y
22	GPCRdb	L193A	Deleterious (61%)	Pathogenic (0.91)	Disease (0.64)	Y
23	rs775861746	T229S	Deleterious (61%)	Pathogenic (0.88)	Disease (0.59)	Y

24	rs771165694	V234M	Deleterious (52%)	Pathogenic (0.98)	Neutral (0.46)	Y
25	rs780853081	I243M	Deleterious (51%)	Pathogenic (0.91)	Neutral (0.47)	Y
26	rs768033952	A248T	Deleterious (61%)	Pathogenic (0.93)	Disease (0.51)	Y
27	rs146828007	V249M	Deleterious (52%)	Pathogenic (0.88)	Neutral (0.48)	Y
28	rs267601158	L252F	Deleterious (61%)	Pathogenic (0.94)	Disease (0.54)	Y
29	GPCRdb	Y275I	Deleterious (55%)	Pathogenic (0.97)	Disease (0.56)	Y
30	rs773478911	M337V	Deleterious (51%)	Pathogenic (0.98)	Neutral (0.45)	Y
31	GPCRdb	D338N	Deleterious (61%)	Pathogenic (0.88)	Disease (0.63)	Y
32	GPCRdb	L341A	Deleterious (61%)	Pathogenic (0.89)	Disease (0.61)	Y
33	rs201203762	A342V	Deleterious (61%)	Pathogenic (0.89)	Disease (0.6)	Y
34	GPCRdb	A342L	Deleterious (61%)	Pathogenic (0.95)	Disease (0.6)	Y
35	rs755954769	A407T	Deleterious (72%)	Pathogenic (0.96)	Neutral (0.44)	Y
36	rs143455045	R409P	Deleterious (65%)	Pathogenic (0.8)	Disease (0.78)	Y
37	rs370158252	K2N	Deleterious (52%)	Pathogenic (0.9)	Neutral (0.26)	N
38	rs748988990	I4T	Deleterious (51%)	Pathogenic (0.88)	Neutral (0.14)	N
39	rs777561684	G7D	Deleterious (61%)	Pathogenic (0.99)	Disease (0.62)	N
40	rs781222994	R14C	Deleterious (52%)	Pathogenic (0.96)	Disease (0.71)	N
41	rs142010122	R14H	Deleterious (76%)	Pathogenic (0.89)	Disease (0.7)	N
42	rs142010122	R14L	Deleterious (87%)	Pathogenic (0.91)	Disease (0.64)	N
43	rs761029757	S25L	Deleterious (52%)	Pathogenic (0.83)	Disease (0.67)	N
44	rs752959680	N26S	Deleterious (72%)	Pathogenic (0.88)	Disease (0.67)	N
45	rs143181991	Y30H	Deleterious (72%)	Pathogenic (0.98)	Disease (0.67)	N
46	rs770413069	E31K	Deleterious (51%)	Pathogenic (0.84)	Disease (0.69)	N
47	rs747979286	Y43C	Deleterious (72%)	Pathogenic (0.83)	Disease (0.61)	N
48	rs267601157	H302P	Deleterious (87%)	Pathogenic (0.93)	Disease (0.93)	N
49	rs267601156	R307C	Deleterious (72%)	Pathogenic (0.92)	Disease (0.81)	N
50	rs112733260	M308T	Deleterious (51%)	Pathogenic (0.98)	Disease (0.51)	N
51	rs538741714	R311C	Deleterious (76%)	Pathogenic (0.94)	Disease (0.79)	N
52	rs766645201	R331Q	Deleterious (87%)	Pathogenic (0.87)	Disease (0.72)	N
53	rs751552163	R331W	Deleterious (87%)	Pathogenic (0.88)	Disease (0.72)	N

54	rs764500177	G417C	Deleterious (55%)	Pathogenic (0.87)	Neutral (0.49)	N
55	rs773947953	S462F	Deleterious (72%)	Pathogenic (0.79)	Disease (0.61)	N
56	rs138027855	T467M	Deleterious (65%)	Pathogenic (0.91)	Neutral (0.15)	N
57	rs868453459	E106K	Neutral (83%)	Pathogenic (0.95)	Neutral (0.47)	Y
58	GPCRdb	Q115A	Neutral (63%)	Pathogenic (0.89)	Neutral (0.43)	Y
59	rs967383969	T125M	Neutral (65%)	Pathogenic (0.91)	Neutral (0.47)	Y
60	rs200255239	G127S	Neutral (63%)	Pathogenic (0.97)	Disease (0.62)	Y
61	rs570687215	H143L	Neutral (60%)	Pathogenic (0.76)	Neutral (0.46)	Y
62	rs780608074	R145S	Neutral (63%)	Pathogenic (0.9)	Disease (0.57)	Y
63	rs143463104	R145H	Neutral (83%)	Pathogenic (0.91)	Disease (0.53)	Y
64	rs751031679	S146R	Neutral (83%)	Pathogenic (0.8)	Neutral (0.48)	Y
65	rs776821613	L164F	Neutral (63%)	Pathogenic (0.94)	Neutral (0.48)	Y
66	rs77016054	S167G	Neutral (83%)	Pathogenic (0.88)	Disease (0.61)	Y
67	GPCRdb	F177A	Neutral (60%)	Pathogenic (0.9)	Disease (0.66)	Y
68	GPCRdb	H181A	Neutral (63%)	Pathogenic (0.93)	Neutral (0.47)	Y
69	rs868306589	R182H	Neutral (74%)	Pathogenic (0.91)	Neutral (0.34)	Y
70	GPCRdb	R182A	Neutral (83%)	Pathogenic (0.96)	Neutral (0.47)	Y
71	GPCRdb	K183A	Neutral (74%)	Pathogenic (0.85)	Neutral (0.39)	Y
72	GPCRdb	D184A	Neutral (60%)	Pathogenic (0.93)	Disease (0.65)	Y
73	rs529665509	S185G	Neutral (83%)	Pathogenic (0.82)	Neutral (0.49)	Y
74	rs201138255	V188M	Neutral (83%)	Pathogenic (0.87)	Neutral (0.46)	Y
75	GPCRdb	F191L	Neutral (83%)	Pathogenic (0.97)	Neutral (0.47)	Y
76	GPCRdb	K192Q	Neutral (60%)	Pathogenic (0.92)	Disease (0.66)	Y
77	GPCRdb	K192R	Neutral (75%)	Pathogenic (0.89)	Neutral (0.4)	Y
78	GPCRdb	L193I	Neutral (83%)	Pathogenic (0.87)	Neutral (0.44)	Y
79	GPCRdb	G195S	Neutral (83%)	Pathogenic (0.95)	Disease (0.62)	Y
80	GPCRdb	A198M	Neutral (75%)	Pathogenic (0.89)	Neutral (0.38)	Y
81	GPCRdb	S199T	Neutral (83%)	Pathogenic (0.88)	Neutral (0.47)	Y
82	rs151214105	I243T	Neutral (63%)	Pathogenic (0.98)	Neutral (0.49)	Y
83	rs771382565	I271T	Neutral (63%)	Pathogenic (0.98)	Neutral (0.5)	Y

84	GPCRdb	V282F	Neutral (63%)	Pathogenic (0.87)	Disease (0.59)	Y
85	rs779516787	V291M	Neutral (75%)	Pathogenic (0.78)	Neutral (0.46)	Y
86	rs750147244	A293V	Neutral (63%)	Pathogenic (0.9)	Neutral (0.46)	Y
87	rs765649111	R340M	Neutral (63%)	Pathogenic (0.97)	Disease (0.71)	Y
88	rs143530073	V364M	Neutral (60%)	Pathogenic (0.87)	Disease (0.54)	Y
89	rs868729092	D366N	Neutral (60%)	Pathogenic (0.92)	Neutral (0.47)	Y
90	rs764560714	T377M	Neutral (60%)	Pathogenic (0.9)	Neutral (0.31)	Y
91	rs149335541	R409W	Neutral (74%)	Pathogenic (0.8)	Neutral (0.44)	Y
92	rs765378853	S410N	Neutral (83%)	Pathogenic (0.81)	Neutral (0.42)	Y
93	rs537218316	F412C	Neutral (63%)	Pathogenic (0.82)	Disease (0.53)	Y
94	rs759024309	P113S	Neutral (74%)	Unknown (0.78)	Neutral (0.48)	Y
95	GPCRdb	S114A	Neutral (83%)	Unknown (0.66)	Neutral (0.18)	Y
96	rs761375736	A120S	Neutral (75%)	Unknown (0.66)	Neutral (0.45)	Y
97	rs774265775	E133G	Neutral (60%)	Unknown (0.8)	Neutral (0.39)	Y
98	rs755180172	V140I	Neutral (71%)	Unknown (0.65)	Neutral (0.42)	Y
99	rs368199704	G157R	Deleterious (87%)	Unknown (0.78)	Disease (0.74)	Y
100	rs368199704	G157S	Deleterious (87%)	Unknown (0.6)	Neutral (0.46)	Y
101	rs747302947	V168A	Neutral (75%)	Unknown (0.74)	Disease (0.5)	Y
102	rs771076412	R186L	Neutral (60%)	Unknown (0.64)	Neutral (0.46)	Y
103	rs771076412	R186H	Neutral (83%)	Unknown (0.53)	Neutral (0.46)	Y
104	GPCRdb	V188A	Neutral (63%)	Unknown (0.76)	Neutral (0.49)	Y
105	rs772388346	P231T	Neutral (83%)	Unknown (0.46)	Neutral (0.24)	Y
106	rs778127844	L239M	Neutral (74%)	Unknown (0.57)	Neutral (0.43)	Y
107	GPCRdb	C257S	Deleterious (61%)	Unknown (0.76)	Disease (0.85)	Y
108	GPCRdb	C264S	Deleterious (87%)	Unknown (0.75)	Disease (0.86)	Y
109	rs749555801	T274S	Neutral (83%)	Unknown (0.72)	Neutral (0.36)	Y
110	rs140051374	G281R	Deleterious (87%)	Unknown (0.82)	Disease (0.84)	Y
111	rs199892728	V285I	Neutral (83%)	Unknown (0.54)	Neutral (0.47)	Y
112	GPCRdb	F289V	Neutral (63%)	Unknown (0.77)	Disease (0.55)	Y
113	rs779516787	V291L	Neutral (60%)	Unknown (0.68)	Neutral (0.48)	Y
114	rs777129355	V351L	Deleterious (72%)	Unknown (0.78)	Neutral (0.45)	Y

115	GPCRdb	C382A	Neutral (63%)	Unknown (0.59)	Neutral (0.5)	Y
116	GPCRdb	C386M	Deleterious (76%)	Unknown (0.8)	Neutral (0.3)	Y
117	GPCRdb	C386A	Neutral (63%)	Unknown (0.63)	Neutral (0.34)	Y
118	rs143455045	R409Q	Deleterious (65%)	Unknown (0.67)	Neutral (0.5)	Y
119	rs773682661	S3L	Neutral (83%)	Pathogenic (0.94)	Neutral (0.27)	N
120	rs75770301	D10N	Neutral (61%)	Pathogenic (0.87)	Disease (0.57)	N
121	rs747886813	F13V	Neutral (83%)	Pathogenic (0.97)	Disease (0.69)	N
122	rs191458319	M62T	Neutral (75%)	Pathogenic (0.88)	Disease (0.68)	N
123	GPCRdb	C98A	Neutral (60%)	Pathogenic (0.81)	Neutral (0.36)	N
124	rs140913272	R307H	Neutral (60%)	Pathogenic (0.88)	Disease (0.68)	N
125	rs750508548	Q310H	Neutral (74%)	Pathogenic (0.79)	Neutral (0.48)	N
126	rs777110971	R311H	Neutral (63%)	Pathogenic (0.89)	Disease (0.57)	N
127	rs147179602	G312D	Neutral (60%)	Pathogenic (0.88)	Neutral (0.47)	N
128	rs757942881	I318S	Neutral (71%)	Pathogenic (0.92)	Neutral (0.45)	N
129	rs753881911	K326N	Neutral (63%)	Pathogenic (0.81)	Neutral (0.47)	N
130	rs764062259	Q328E	Neutral (75%)	Pathogenic (0.8)	Neutral (0.44)	N
131	rs749116792	C431Y	Neutral (63%)	Pathogenic (0.9)	Disease (0.53)	N
132	rs760079776	T453K	Neutral (60%)	Pathogenic (0.90)	Neutral (0.4)	N
133	rs765964116	V463A	Neutral (65%)	Pathogenic (0.79)	Neutral (0.12)	N
134	rs748988990	I4N	Neutral (83%)	Unknown (0.69)	Disease (0.57)	N
135	rs747783434	L21Q	Neutral (83%)	Unknown (0.69)	Neutral (0.27)	N
136	rs148575019	V23M	Neutral (83%)	Unknown (0.4)	Neutral (0.11)	N
137	rs768086951	D27G	Deleterious (55%)	Unknown (0.82)	Disease (0.7)	N
138	rs1021828541	I33M	Neutral (83%)	Unknown (0.4)	Neutral (0.49)	N
139	rs201496665	K34R	Neutral (75%)	Unknown (0.56)	Neutral (0.49)	N
140	rs138753523	M37I	Neutral (83%)	Unknown (0.62)	Neutral (0.12)	N
141	rs780977671	A38T	Neutral (75%)	Unknown (0.58)	Disease (0.64)	N
142	rs1011805931	G42R	Deleterious (55%)	Unknown (0.64)	Disease (0.71)	N
143	rs780029930	G55A	Neutral (75%)	Unknown (0.5)	Neutral (0.08)	N
144	rs370946660	G55R	Neutral (75%)	Unknown (0.54)	Neutral (0.13)	N
145	rs753845620	Q59R	Neutral (74%)	Unknown (0.53)	Disease (0.63)	N

146	rs756276407	T63P	Neutral (74%)	Unknown (0.64)	Neutral (0.37)	N
147	rs767810773	A64V	Neutral (74%)	Unknown (0.42)	Neutral (0.5)	N
148	rs752064133	N67S	Neutral (83%)	Unknown (0.36)	Neutral (0.08)	N
149	rs752064133	N67T	Neutral (83%)	Unknown (0.37)	Neutral (0.16)	N
150	rs762584169	Q69P	Neutral (74%)	Unknown (0.63)	Disease (0.72)	N
151	rs772800072	A73P	Neutral (75%)	Unknown (0.4)	Neutral (0.49)	N
152	rs761413185	D74G	Neutral (63%)	Unknown (0.46)	Disease (0.51)	N
153	rs746763924	V76L	Neutral (83%)	Unknown (0.37)	Neutral (0.12)	N
154	rs771953798	I78T	Neutral (65%)	Unknown (0.47)	Neutral (0.31)	N
155	rs201771485	I78V	Neutral (83%)	Unknown (0.31)	Neutral (0.08)	N
156	rs201771485	I78F	Neutral (83%)	Unknown (0.52)	Neutral (0.23)	N
157	rs145855770	L86F	Neutral (75%)	Unknown (0.45)	Neutral (0.3)	N
158	rs756153990	S87L	Deleterious (60%)	Unknown (0.66)	Neutral (0.46)	N
159	rs370383012	S87P	Neutral (52%)	Unknown (0.67)	Neutral (0.37)	N
160	rs372334867	S88F	Neutral (65%)	Unknown (0.65)	Neutral (0.23)	N
161	rs570301594	K90R	Neutral (83%)	Unknown (0.59)	Neutral (0.14)	N
162	rs202238406	E93K	Neutral (74%)	Unknown (0.64)	Neutral (0.41)	N
163	rs200550971	Q97R	Neutral (75%)	Unknown (0.66)	Neutral (0.37)	N
164	rs1004049036	Q97H	Neutral (83%)	Unknown (0.69)	Neutral (0.3)	N
165	rs766443788	A305T	Neutral (65%)	Unknown (0.78)	Neutral (0.46)	N
166	rs568621412	V306I	Neutral (74%)	Unknown (0.72)	Neutral (0.33)	N
167	rs746439921	I317V	Neutral (83%)	Unknown (0.6)	Neutral (0.29)	N
168	rs779790677	I317M	Neutral (83%)	Unknown (0.62)	Neutral (0.38)	N
169	rs371968575	T321K	Deleterious (51%)	Unknown (0.48)	Neutral (0.36)	N
170	rs371968575	T321R	Deleterious (51%)	Unknown (0.64)	Neutral (0.48)	N
171	rs371968575	T321M	Neutral (61%)	Unknown (0.54)	Neutral (0.48)	N
172	rs368681404	T330I	Neutral (83%)	Unknown (0.73)	Neutral (0.18)	N
173	rs754155465	E416K	Neutral (83%)	Unknown (0.57)	Neutral (0.28)	N
174	rs78783387	A419V	Neutral (71%)	Unknown (0.52)	Neutral (0.39)	N
175	rs78783387	A419E	Neutral (74%)	Unknown (0.63)	Neutral (0.29)	N

176	rs771535671	D423N	Neutral (83%)	Unknown (0.61)	Neutral (0.28)	N
177	rs770665729	D430G	Neutral (63%)	Unknown (0.69)	Neutral (0.35)	N
178	rs777759836	K434N	Neutral (63%)	Unknown (0.53)	Neutral (0.19)	N
179	rs769601091	H435Y	Neutral (63%)	Unknown (0.63)	Neutral (0.34)	N
180	rs370487985	A436T	Neutral (83%)	Unknown (0.54)	Neutral (0.21)	N
181	rs758413605	V442G	Neutral (74%)	Unknown (0.65)	Neutral (0.46)	N
182	rs750464422	R444G	Deleterious (51%)	Unknown (0.78)	Disease (0.54)	N
183	rs772492894	A446T	Neutral (60%)	Unknown (0.79)	Neutral (0.21)	N
184	rs772492894	A446S	Neutral (83%)	Unknown (0.67)	Neutral (0.21)	N
185	rs764437215	I450T	Neutral (74%)	Unknown (0.80)	Neutral (0.22)	N
186	rs951061482	I450V	Neutral (83%)	Unknown (0.49)	Neutral (0.06)	N
187	rs756483875	S452T	Neutral (83%)	Unknown (0.61)	Neutral (0.18)	N
188	rs141056981	I456V	Neutral (83%)	Unknown (0.54)	Neutral (0.06)	N
189	rs375652364	V459I	Neutral (74%)	Unknown (0.70)	Neutral (0.05)	N
190	rs768591630	A471S	Neutral (63%)	Unknown (0.70)	Neutral (0.2)	N